A COMBINED NUMERICAL AND EXPERIMENTAL INVESTIGATION OF THE EFFECTS OF BURIED EXPLOSIVE CHARGES

R. T. Sedgwick, et al

Systems, Science and Software

Prepared for:

Army Mobility Equipment Research and Development Center

September 1974

AD/A 001 744

REPORT DOCUMENTATION PAGE

READ INSTRUCTIONS BEFORE COMPLETING FORM

1 REPORT NUMBER: SSS-R-74-2410	2 GOVT ACCESSION NO.
3 RECIPIENT'S CATALOG NUMBER	
4 TITLE (and Subtitle): A Combined Numerical and Experimental Investigation of the Effects of Buried Explosive Charges	5 TYPE OF REPORT & PERIOD COVERED: Final Report
	6 PERFORMING ORG. REPORT NUMBER: SSS-R-74-2410
7 AUTHOR(s): R. T. Sedgwick, E. S. Gaffney, D. E. Wilkins, L. J. Walsh	8 CONTRACT OR GRANT NUMBER(S): DAAK-02-73-C-0103
9 PERFORMING ORGANIZATION NAME AND ADDRESS: Systems, Science and Software, P. O. Box 1620, La Jolla, CA 92037	10 PROGRAM ELEMENT, PROJECT, TASK AREA & WORK UNIT NUMBERS
11 CONTROLLING OFFICE NAME AND ADDRESS: U.S. Mobility Equipment Research and Development Center, Ft. Belvoir, VA 22060	12 REPORT DATE: September 1974 13 NUMBER OF PAGES: 96
14 MONITORING AGENCY NAME & ADDRESS (if different from Controlling Office)	15 SECURITY CLASS (of this report): Unclassified 15a DECLASSIFICATION/DOWNGRADING SCHEDULE

16 DISTRIBUTION STATEMENT (of this Report)

Unlimited Distribution

17 DISTRIBUTION STATEMENT (of the abstract entered in Block 20, if different from Report)

18 SUPPLEMENTARY NOTES

19 KEY WORDS (Continue on reverse side if necessary and identify by block number)

Buried Mines
High Explosives
Numerical Calculations
Soils
Equation of State
Explosive Effects
Stress Measurement

20 ABSTRACT (Continue on reverse side if necessary and identify by block number)

The two-dimensional HELP computer code has been modified to solve the interaction between buried explosive charges and simple structures located above ground level. Three calculations were performed and the results compared favorably with results from a concurrent test program.

Dynamic material properties experiments were performed to provide the necessary soil equation of state parameters which are required as input to the numerical model.

DD FORM 1 JAN 73 1473 EDITION OF 1 NOV 65 IS OBSOLETE

UNCLASSIFIED (96)

SECURITY CLASSIFICATION OF THIS PAGE (When Data Entered)

Report SSS-R-74-2410

A COMBINED NUMERICAL AND EXPERIMENTAL INVESTIGATION OF THE EFFECTS OF BURIED EXPLOSIVE CHARGES

Final Report

by

R. T. Sedgwick
E. S. Gaffney
D. E. Wilkins
L. J. Walsh

September 1974

Prepared for

U. S. Army Mobility Equipment Research and Development Center
Fort Belvoir, Virginia 22060

Prepared by

Systems, Science and Software
La Jolla, California ..037

Under Contract Number
DAAK-02-73-C-0103

ABSTRACT

The two-dimensional HELP computer code has been modified to solve the interaction between buried explosive charges and simple structures located above ground level. Three calculations were performed and the results compared favorably with results from a concurrent test program.

Dynamic material properties experiments were performed to provide the necessary soil equation of state parameters which are required as input to the numerical model.

ACKNOWLEDGMENTS

The authors wish to acknowledge Mr. Bruce Morris of MERDC for his helpful suggestions and comments during the course of this investigation. In addition, the authors are grateful to Mr. Dave Scott for his cooperation and assistance during our visits to the MERDC Computer Center.

I. INTRODUCTION

Techniques for predicting the effects of buried explosive charges on structures in contact with or above the ground surface are of interest to engineers and designers working in the area of mine warfare technology. The computer code, HELP,[1] has recently been modified[2] to solve two-dimensional, axisymmetric problems involving the detonation of a buried explosive charge, the expansion of the detonated products, the interaction of these gasses with the soil, the acceleration of the soil and its interaction with a flat plate located above the ground and finally, the stress propagation through the plate. The code has been employed in the theoretical portion of a joint theoretical/experimental investigation of buried mine effects and the results of three calculations are presented herein.

The experimental portion of the investigation included basic soil property tests to provide points on the Hugoniot needed for determining input parameters for the numerical model as well as a test program for the purpose of validating the theoretical predictions.

Section II of this report discusses the experimental techniques employed to determine the required soil properties and presents the experimental matrix along with the desired results. Section III describes the test set up and results from the buried explosive charge experiments. In Section IV the results from three calculations are presented and compared with data from the experimental program. Concluding remarks are presented in Section V.

The results reported herein indicate that significant advancement in the state-of-the-art of predictive techniques for evaluating the effects of buried explosive charges has been attained.

II. SOIL PROPERTIES EXPERIMENTS

2.1 INTRODUCTION

Successful application of the computational techniques described earlier[2] depends on the availability of an accurate model of the dynamic behavior of the soil under which the charge is buried. The particular equation of state chosen is that of Tillotson[3] which has the form

$$P = \left[a + \frac{b}{\frac{I}{I_0 \eta^2} + 1} \right] I\rho + A\mu + B\mu^2 \qquad (1)$$

where $\eta = \rho/\rho_0 = \mu + 1$, and ρ_0, a, b, I_0, A, and B are constants. The values of the constants must be determined either by experiment or by analogy with other materials. These parameters will be discussed below after describing the experimental techniques and results.

Two soils, each in two different density-saturation states, were studied. The first soil, McCormick Ranch Sand from near Albuquerque, New Mexico, was chosen because static test data[4] and a limited amount of shock data[5] were already available. The second soil, from Southwest Research Institute near San Antonio, Texas (referred to below as SwRI soil) was chosen because it had been the test medium for previous experiments with buried explosive charges.[6] The "dry" state (ρ_0 = 1.36 gm/cm^3, w = 8.4%) was chosen as the mean state of the wetter (and less dense) of two relatively dry groups of soils used by Wenzel and Esparza.[6] The water content and density of the "wet" McCormick Ranch sand were chosen to be near those

used in previous shock studies[5] (ρ_0 = 2.12 gm/cm^3, w = 12%). The properties of the "wet" SwRI soil were chosen to yield an intermediate density (1.70 gm/cm^3) at the plastic limit (19.4% water).

2.2 MEASUREMENT TECHNIQUES

2.2.1 Static Properties

The plastic limit of the SwRI soil was determined using ASTM D424-59 procedures. The plastic limit of the McCormick Ranch sand was taken to be 14 percent, the water content used by Peterson and Gates.[5] Mazanti and Holland [4] give a plastic limit of 15 percent which is within the accuracy of the technique.

The water content of both materials as received was determined according to ASTM D2216-71 specifications. The SwRI soil had an initial water content greater than 8.4 percent so it was necessary to dry a portion of it to mix with the remainder for the "dry" samples. The water content of the McCormick Ranch sand as received was also 8.4 percent. Each soil was divided into two batches and sufficient water added (if necessary) to bring the water content to the desired amount. Thereafter the soils were stored in sealed plastic bags except when the soil was being extracted for tests. The water content was checked at intervals and found to be stable when stored in this manner.

The desired initial density of test samples was achieved by pressing a known mass of soil into a known volume of sample holder. For the dry soils this could be done by hand, pressing an aluminum anvil on the soil until it rested on the surface of the ring containing the soil. For the wet soils it was necessary to use a hydraulic press to achieve the desired densities. Our past experience has been that this technique leads to density variations of about 5 percent with higher densities at the center of the sample for soils near their plastic limit. Consequently, we used 2 1/2 percent

less soil than that calculated to give the proper density. This procedure gives the desired density in the center of the sample where the gages were located. For dry soils the variation from the desired density is less than one percent.

2.2.2 Dynamic Properties

The dynamic equation of state measurements below 40 kbar were made using the $1.3 cm^3$ light gas gun facility. A projectile, whose front end is a flat plate of standard material, is accelerated in the gun and, upon leaving the barrel, impacts the sample, sending a shock wave into the sample. Gauges are placed in the sample to determine the shock wave velocity and amplitude. Analysis of the event will be described in Section 2.2.3 after describing the experiments in more detail.

Most of the samples in this study were in targets of two configurations. In the first arrangement (Figure 1a) a single layer of the sample material was placed between two layers, one of aluminum and one of plexiglas (pmma). At both interfaces there was a manganin piezoresistive gauge. In order to prevent individual soil particles from piercing the gauges and changing their resistence a layer of epoxy impregnated fiberglas 0.013 cm thick covered the gauges. As we discuss below, this technique was not completely successful. The gauges were connected to a bridge circuit (Pulsar 251A) to monitor their change in resistance as the shock wave passed. The pressure was determined from the known piezoresistive coefficient of manganin, and the shock velocity was determined from the transit time through a known thickness of sample. This configuration was used

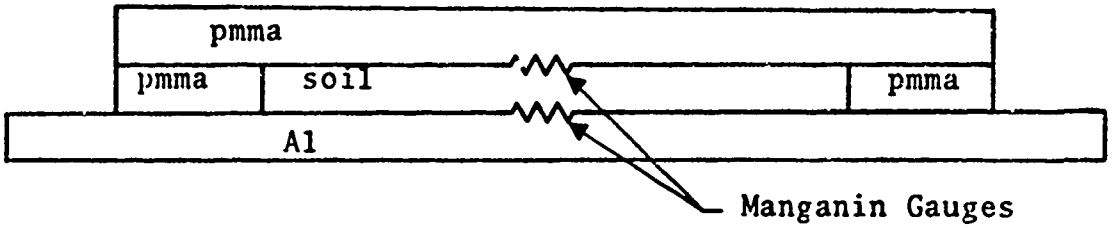

Fig. 1(a)--Single layer soil targets used in gas gun experiments.

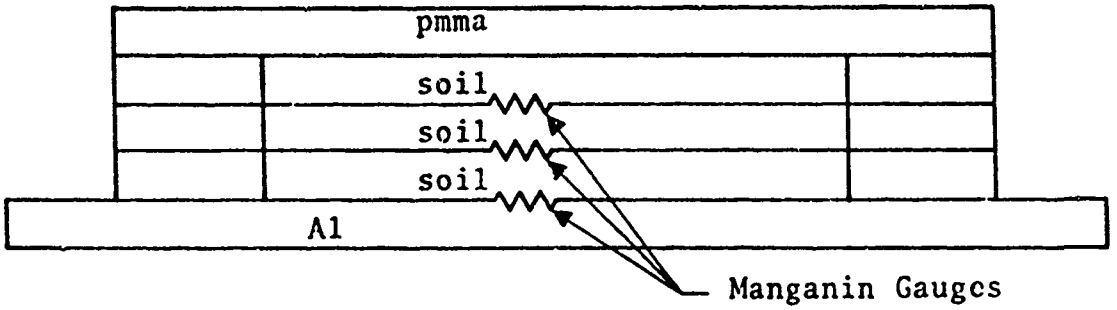

Fig. 1(b)--Multi-layer soil targets used in gas gun experiments.

for the initial experiments on SwRI soil to aid in designing later shots and to determine the approximate equations of state.

Most of the gas gun experiments employed the target configuration shown in Fig. 1b. In these experiments there are three piezoresistive gauges--one between the buffer and the soil and two more in the soil. In one experiment a one-inch thick steel disc which was used as a weight during the sample assembly process, was accidentally glued to the rear surface. Since the steel could not be removed from the specimen without destroying it and since it could not affect the initial loading, the shot was carried out as planned. In this shot (number 204) we were able to determine an approximate second-shock Hugoniot point. Unfortunately, neither the type of steel nor its heat treatment was known so there are considerable errors attached to that datum.

Our original intention had been to perform several experiments using explosively launched plates to obtain equation of state data in the range from 50 to 150 kbar. Because of problems with gauge survival only one such experiment was performed. The experimental arrangement is shown in Fig. 2. The gauges and recording procedures were similar to those in the gas gun experiments.

Most of the data reported below were evaluated using impedance matching techniques. In cases where the pressure calculated from impedance matching using the observed shock velocity disagreed markedly from that measured by the manganin gauges, the former was accepted as correct. In all such cases the measured stresses were too high and it is thought that this was due to the stretching of the gauge as it is impacted

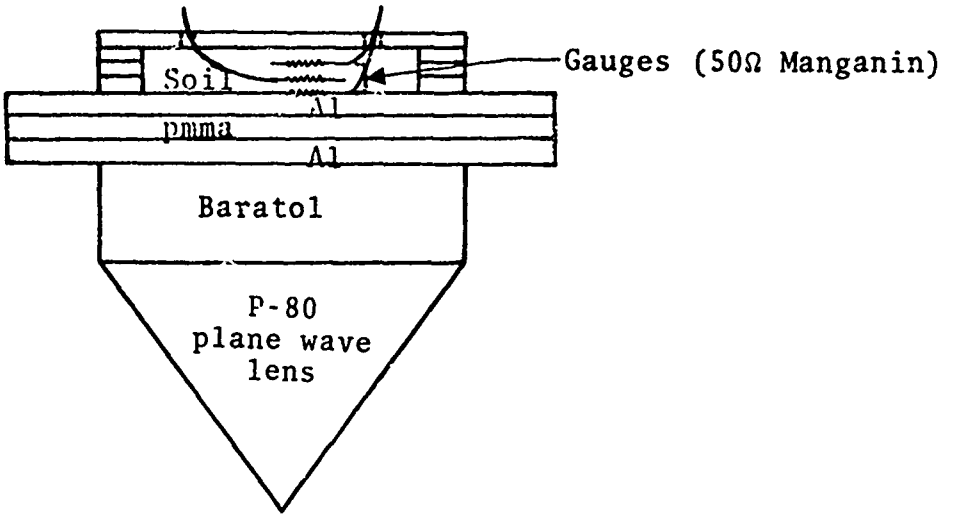

Fig. 2--Experimental arrangement for high explosive equation of state measurements.

by the individual grains in the soil. Such deformation is a common problem in application of piezoresistive gauges to granular materials. A variety of encapsulating media including kapton, mylar and epoxy impregnated fiberglass were investigated to try to prevent this. None proved completely successful but the best results were obtained with the fiberglass packages.

The records from one experiment were apparently unaffected by gauge stretching in as much as the measured and inferred stresses were nearly identical. Furthermore, the wave did not attenuate appreciably between the first two gauges. These records were analysed by the Lagrangian gauge analysis scheme of Fowles and Williams.[7] The computer program for this analysis (GAGES) was supplied by Stanford Research Institute.

2.3 RESULTS

2.3.1 McCormick Ranch Sand

A total of eleven gas gun experiments were performed on McCormick Ranch sand. Two were technique shots which produced no useful data. Two failed due to bad projectile design and on a fifth shot, scopes misfired. One shot provided both direct shock data and reflected shot data so that, in effect, there were seven successful experiments.

The available Hugoniot data on McCormick Ranch sand are tabulated in Table I. The three experiments at low stresses are taken from Peterson and Gates.[5]

One of the points (p = 32.5 kbars) in Table I is the final state from a Lagrangian gauge analysis of a pair of stress-time records as mentioned above.

TABLE I

MCCORMICK RANCH SAND

P	U	D	ρ_H	V_H	w	ρ_0	$V_H{}_2O$	V_s
0.19	0.049	0.32	1.75	0.5714	0	1.48	-	0.571
0.6	0.072	0.54	1.71	0.5848	0	1.48	-	0.585
1.5	0.060	1.17	2.23	0.4484	0.12	2.12	0.944	0.379
7.36	0.512	1.06	2.64	0.3788	0.085	1.36	0.843	0.339
12.0	0.617	1.43	2.39	0.4184	0.085	1.36	0.804	0.386
26.8	0.500	2.53	2.64	0.3788	0.12	2.12	0.731	0.330
27.4	0.483	2.68	2.59	0.3861	0.12	2.12	0.29	0.338
32.5	0.620	2.47	2.83	0.3535	0.12	2.12	0.714	0.303
33.3	0.575	2.75	2.68	0.3731	0.12	2.12	0.712	0.326
(58)	(0.88)	(3.1)	(2.96)	(0.338)	0.12	2.12	0.660	(0.293)

P = Hugoniot pressure (kbar)

U = Particle velocity (mm/μsec)

D = Shock velocity (mm/μsec)

ρ_H = Hugoniot density (gm/cm^3)

V_H = Hugoniot volume = $1/\rho_H$ (cm^3/gm)

w = Water content by dry weight (percent)

ρ_0 = Initial density (gm/cm^3)

V_{H_2O} = Specific volume of water at $P = P_H$ (cm^3/gm)

V_s = Specific volume of solids (cm^3/gm)

Data in parentheses ( ) is for a doubly shocked state.

2.3.2 Southwest Research Institute (SwRI) Soil

Six light gas gun shots and one high explosive experiment were performed on SwRI soil. Two of the gas gun shots yielded both Hugoniot and reflected shock data, but three resulted in no usable data. These results are tabulated in Table II.

2.4 DISCUSSION

2.4.1 Experimental Problems in Studying Shocked Soils

Soils are extremely complex composites of voids, water, and (usually) several solid phases (predominately silicates). Because the various components have markedly different impedences, the shock front in a soil will be highly convoluted on the scale of individual grains. Furthermore, just behind the front of the wave there will be large velocity gradients until the components have reached mechanical equilibrium. This feature makes it very difficult to use in-material gauges in soils. Thin foil gauges are chopped and sliced by the passage of a shock front. Encapsulating the gauges in sheet material, such as mylar, kapton or fiberglass improves their performance but not enough to permit the use of piezoresistive gauges in dry soils. Even if these materials prevent the actual cutting of the gauge element by the soil particles they often will not prevent stretching. Either cutting or stretching of the piezoresistive element will give anomalously high stress readings such as were seen in many of the shots reported here.

The use of either ytterbium piezoresistive gauges or magnetic particle velocity gauges has been suggested to alleviate this problem. Ytterbium, with a higher piezoresistive coefficient than manganin, will give a larger signal at a given stress, so that the anomalous signal due to stretching will be relatively smaller. This is not a feasible solution at high

TABLE II

SwRI SOIL

P	U	D	ρ_H	V_H	$M_H^2 0$	ρ_0	$V_H^2 0$	V_s
4.24	0 24	1.3	1.67	0.5995	0.085	1.36	0.883	0.575
7.3	0.465	1.15	2.28	0.4390	0.085	1.36	0.843	0.405
12.6	0.424	1.75	2.24	0.4456	0.194	1.70	0.800	0.377
14.5	0.467	1.83	2.28	0.4378	0.194	1.70	0.789	0.370
(52 ±5)	(0.87 ±.03)	(3.52 ±.42)	(2.26)	(0.443)	0.194	1.70	(0.669)	(0.399)

Symbols as in Table 1. Data in parentheses() are from high explosive shot and may have considerable errors

pressures since ytterbium is very [illegible] rather than deform plastically. Another, but less promising, approach is to try still other encapsulating media. Certainly the gauge can be protected by very thick sheets on the order of 1/16 inch, but in that case the effect of the gauge package on the shock propagation will be great unless there is a good impedence match between the soil and the gage.

Perhaps the most promising solution is the use of in-material magnetic velocity gauges. Since these gauges can have low initial resistance without losing signal level, they can be made of thick enough material to withstand the velocity gradients in soils. The main difficulty with these gauges is the requirement that moving conductors must remain remote from the target and this limits the impedence of flyers that can be used.

2.4.2 Calculation of Poreless McCormick Ranch Sand Properties

In order to interpret the above data, obtained from different soils and water contents, in a unified manner let us use a simple mixture theory to extract the "Hugoniot" of the solids from the soil results. To do this we assume complete pore collapse and assume that the water (if present) and the solids both attain the specific volume appropriate to the separate phases at the pressure attained in the soil.

Symbolically,

$$V_H(P) = \left(V_s(P) + M_w V_w(P)\right) / \left(1 + M_w\right) \qquad (2)$$

where $V_H(P)$, $V_s(P)$, and $V_w(P)$ are the specific volume of the soil, solids, and water, respectively, shocked to pressure P and M_w is the water content in percent of dry weight. The Hugoniot of water, shown in Figure 3b, is a combination of data by Lysne[8] and the tabulation of Riney, et al.[9] Then

$$V_s(P) = \left(1 + M_w\right) V_H(P) - M_w V_w(P) \qquad (3)$$

We have done this calculation for all the data available on these two soils and the resulting volume of solids is shown as a function of Hugoniot pressure in Fig. 3.

All of the McCormick Ranch sand data above 1 kbar lie near the line $V_s(P) = 0.382 - 0.0019P$ where V has the units of cc/gm and P is in kbars. We take this to indicate that closing of pores in this material takes place at very low stresses. By using this expression for $V_s(P)$ we show below that we can fit most of the data well in the shock velocity-particle velocity plane.

The data for the SwRI soil all lie to the right of the line used to represent McCormick Ranch sand as seen in Figure 3. For the wet soil the deviation is within the scatter of the data for the McCormick Ranch sand alone. However, if we consider the difference to be real then two interpretations are possible. The Hugoniot of the solids may be the same as in McCormick Ranch sand, but the SwRI soil may resist complete pore collapse to fairly high pressures. Alternately the solids in the SwRI soil may be stiffer. We show the Hugoniot for a pure quartz rock[10] as an example. Even in this case we must conclude that the dry SwRI soil does not collapse until at least 7-8 kbar.

2.4.3 Implication of Poreless McCormick Ranch Sand

If we use Eq. (2) and the curves in Figs. 3a and 3b we can calculate the expected Hugoniots for the void-free water bearing soils shown in Fig. 4. Solid curves are for the McCormick Ranch sand solids. Curves are shown for all of the water contents shown in Tables I and II and each data point is connected to the appropriate curve by a straight line. A comparison of the calculated void-free Hugoniots with experimental data allows one to estimate the degree of pore collapse that has occurred in the soil.

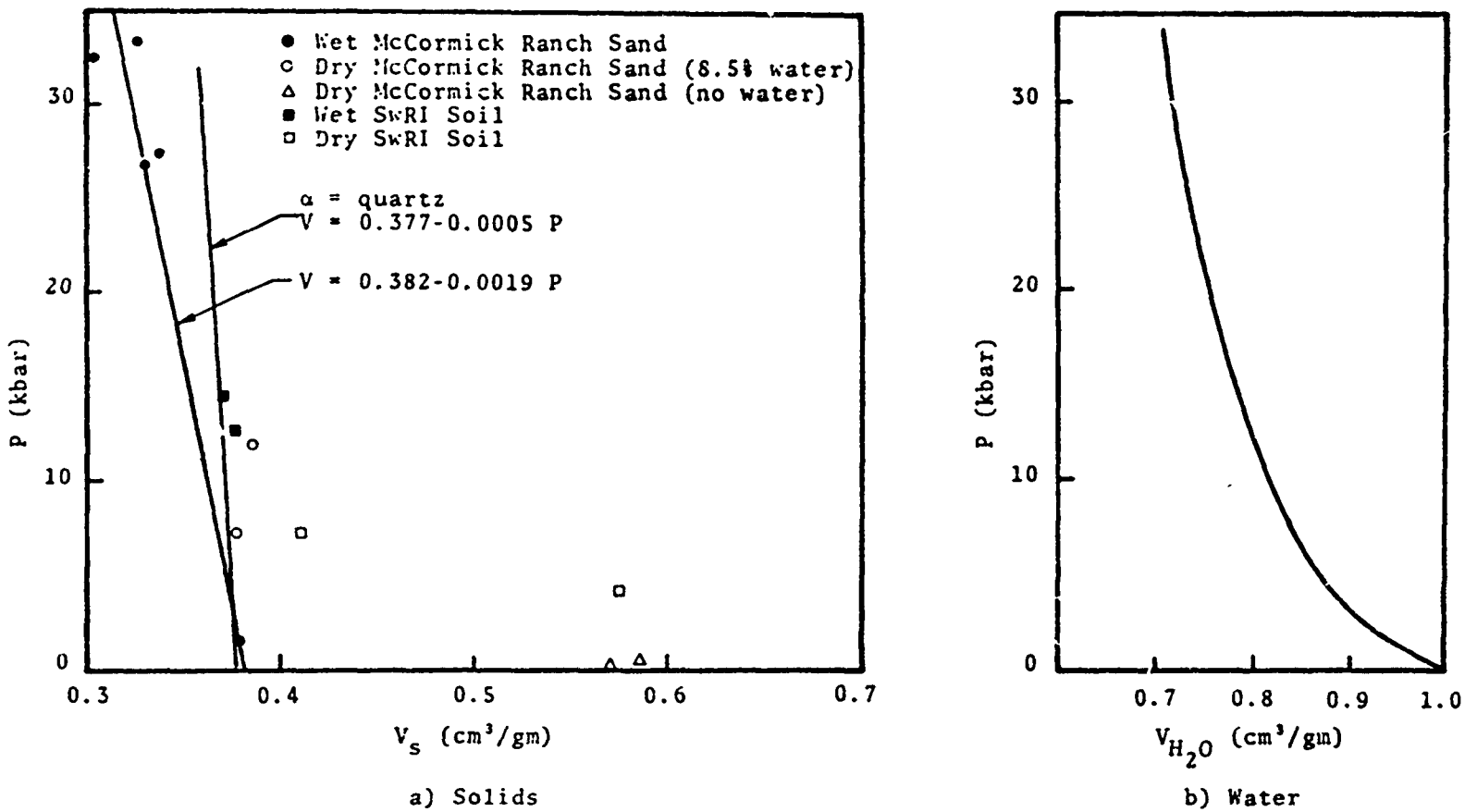

Fig. 3--Hugoniot of solids in soils and of water

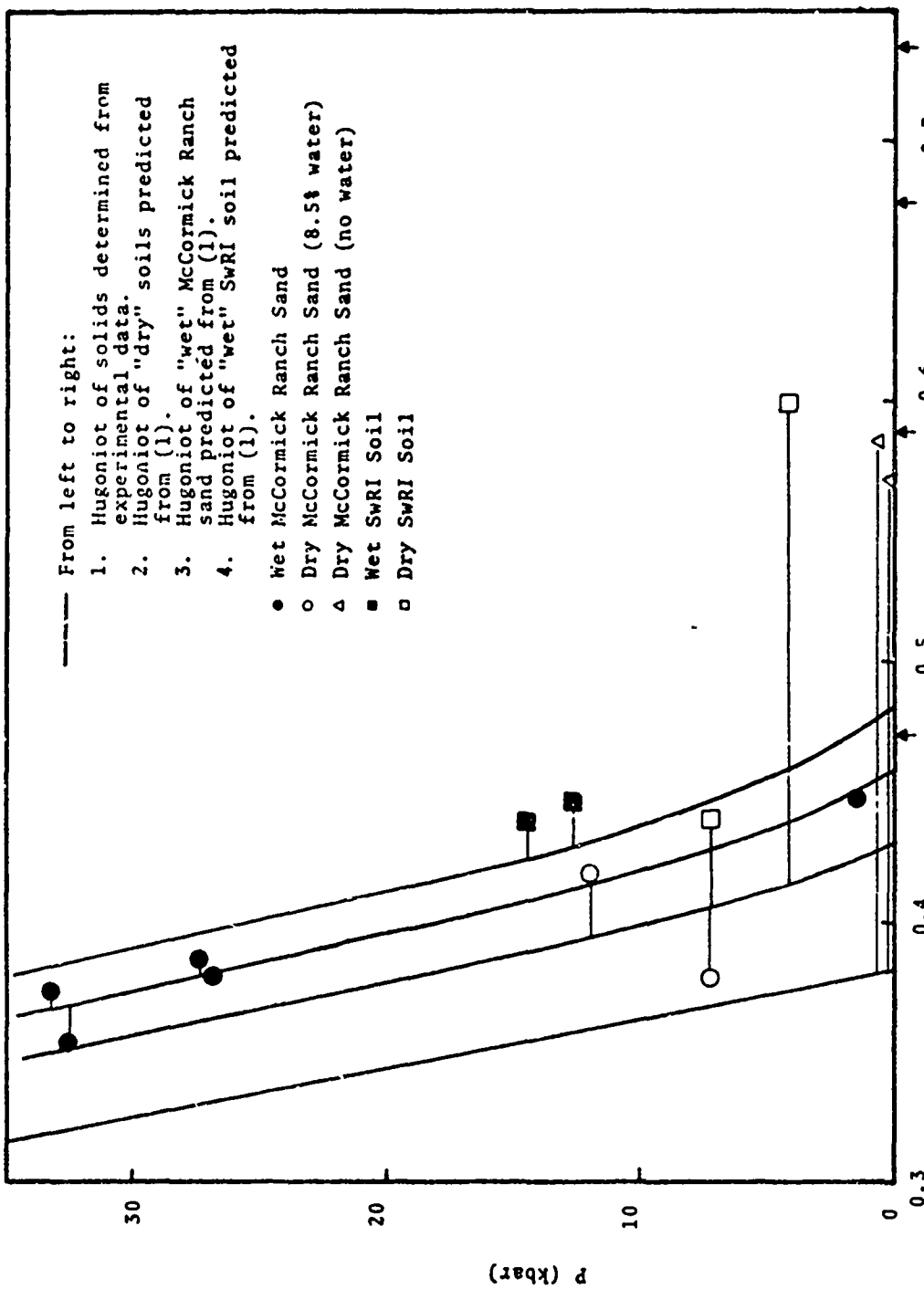

Fig. 4--Hugoniot data and derived Hugoniot curves for five soils.

The same data as in Fig. 4 are shown in particle velocity-shock velocity space in Fig. 5. In this figure we have also indicated the zero pressure sound speed for McCormich Ranch sand calculated from the hydrostatic compression curve.[4] There is excellent agreement between the observations and the curve shown. Also shown is the linear D-U relation which has been used for the NTS Playa soil discussed in Subsection 2.4.4. As can be seen, it is in good agreement with our 30 kbar data on McCormick Ranch sand but agreement is poor at lower pressures.

The very high compressibility shown by the solids in McCormick Ranch sand up to 35 kbars cannot be used to estimate $V_s(P)$ for very high pressures. The scatter of the data in Fig. 4 is sufficient to preclude an estimate of the curvature. Nonetheless, we can be certain that before stresses of 100 kbar are reached the curvature would become evident. Because of the high initial compressibility we should expect the effect to be fairly pronounced.

The very high initial compressibility of the solids in McCormick Ranch sand may indicate that there is more water in the samples than supposed. Inter-lamellar water in clay minerals might account for such an effect. This water is often difficult to remove completely at moderate temperatures. We would expect clean sands to be stiffer as, indeed, they are.

Using the curves of Fig. 3 we can derive the parameters A and B of the Tillotson equation. The first term is not important at the stress levels studied here. Values of a, b and I_o have been chosen so that the terms $a + b / (I/I_o\eta^2 + 1)$ equals a typical Gruneisen parameter for soils. The values are given in Table III.

2.4.4 Revised Equation of State of NTS Playa Soil

At very high stresses (in excess of 100 kbar) we expect that the silicates in the soil will transform to new structures with silicon in six coordination with oxygen instead

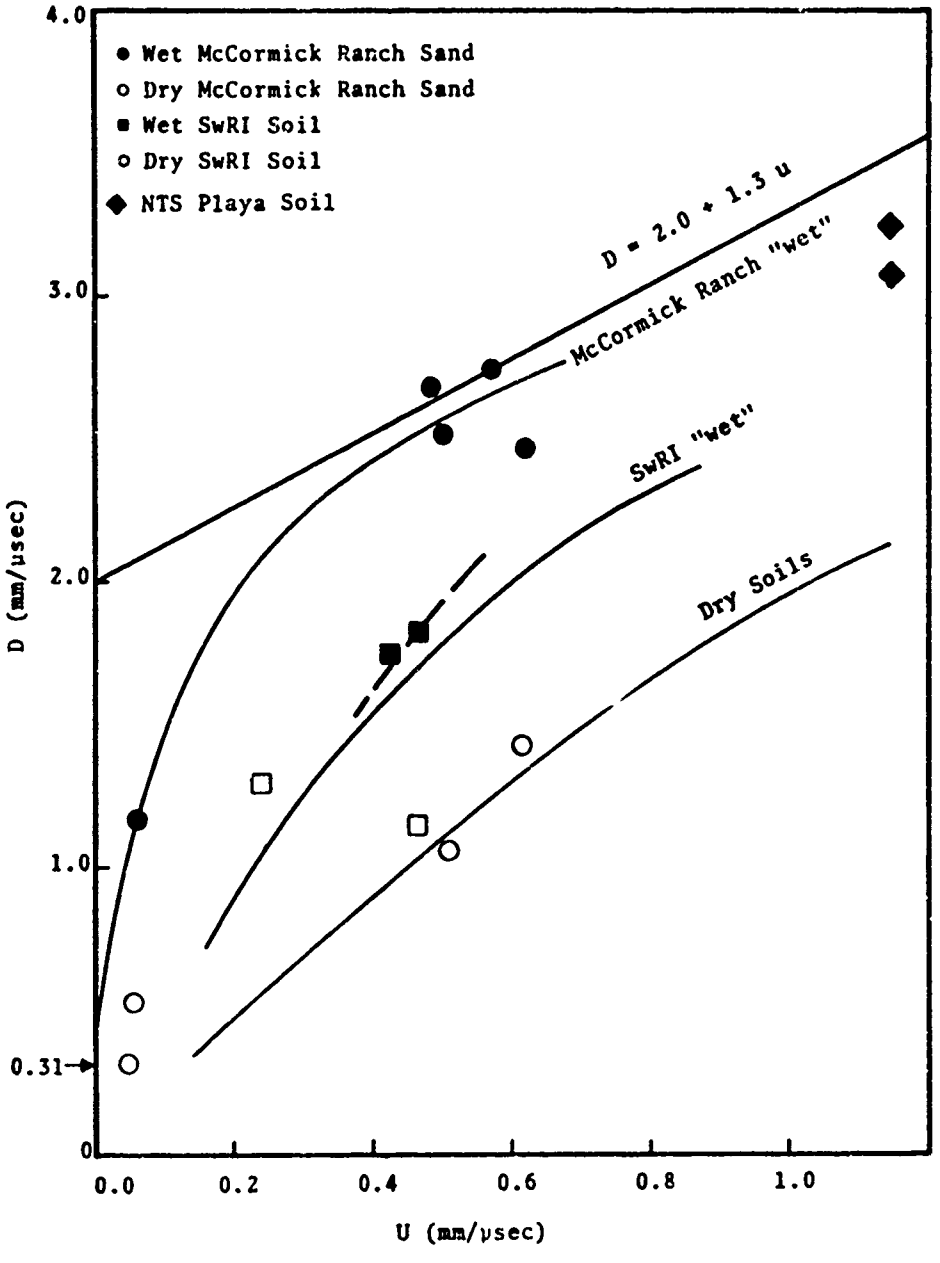

Fig. 5--Hugoniot of four soils in shock velocity (D)--particle velocity (U) space, → zero pressure sound speed of wet McCormick Ranch Sand.[4]

TABLE III

TILLOTSON EQUATION OF STATE PARAMETERS FOR
WET MC CORMICK RANCH SAND

$A = 5.1 \times 10^{9}$ dynes/cm^2

$B = 4.576 \times 10^{11}$ dynes/cm^2

$a = 0.1$

$b = 0$

$I_o = 1$ erg/g

$\rho_o = 2.12$ g/cm^3

of the normal four coordination. Such structures have been observed in most silicates that have been studied.[10-13] In light of this possibility we have reassessed the equation of state of NTS playa soil used in our earlier reports. The revised equation of state is shown schematically in Fig. 6. We have assumed that a phase change occurs between 150 kbar and 250 kbar. The result is a much closer fit to the experimental data that also agrees with predictions based on crystal chemical considerations and previous experience with silicates. Although we have not done so here, it would be possible to use Eq. (3) to determine the equation of state of the solids in the NTS playa soil to determine how they compare with available data on silicates.

2.5 CONCLUSIONS AND RECOMMENDATIONS

This investigation of the dynamic properties of two soils has led to the following conclusions:

- A simple mixture theory can be applied consistently to the equation of state of McCormick Ranch sand in three states of porosity and saturation, two from the present study and one from ref. 5.
- The solids in McCormick Ranch sand show an apparent initial density of 2.62 gm/cm^3 and an apparent initial bulk modulus of 200 kbar.
- In incompletely saturated McCormick Ranch sand (ρ_0 = 1.36 gm/cm^3, w = 8.5 percent dry weight) collapse of pore volume occurs at a stress less than 7 kbar.
- Completely dry McCormick Ranch sand has open pore space at pressures at least as high as 0.6 kbar.
- Within experimental uncertainty Southwest Research Institute (SwRI) soil has an equation of state consistent with the same solids as inferred for

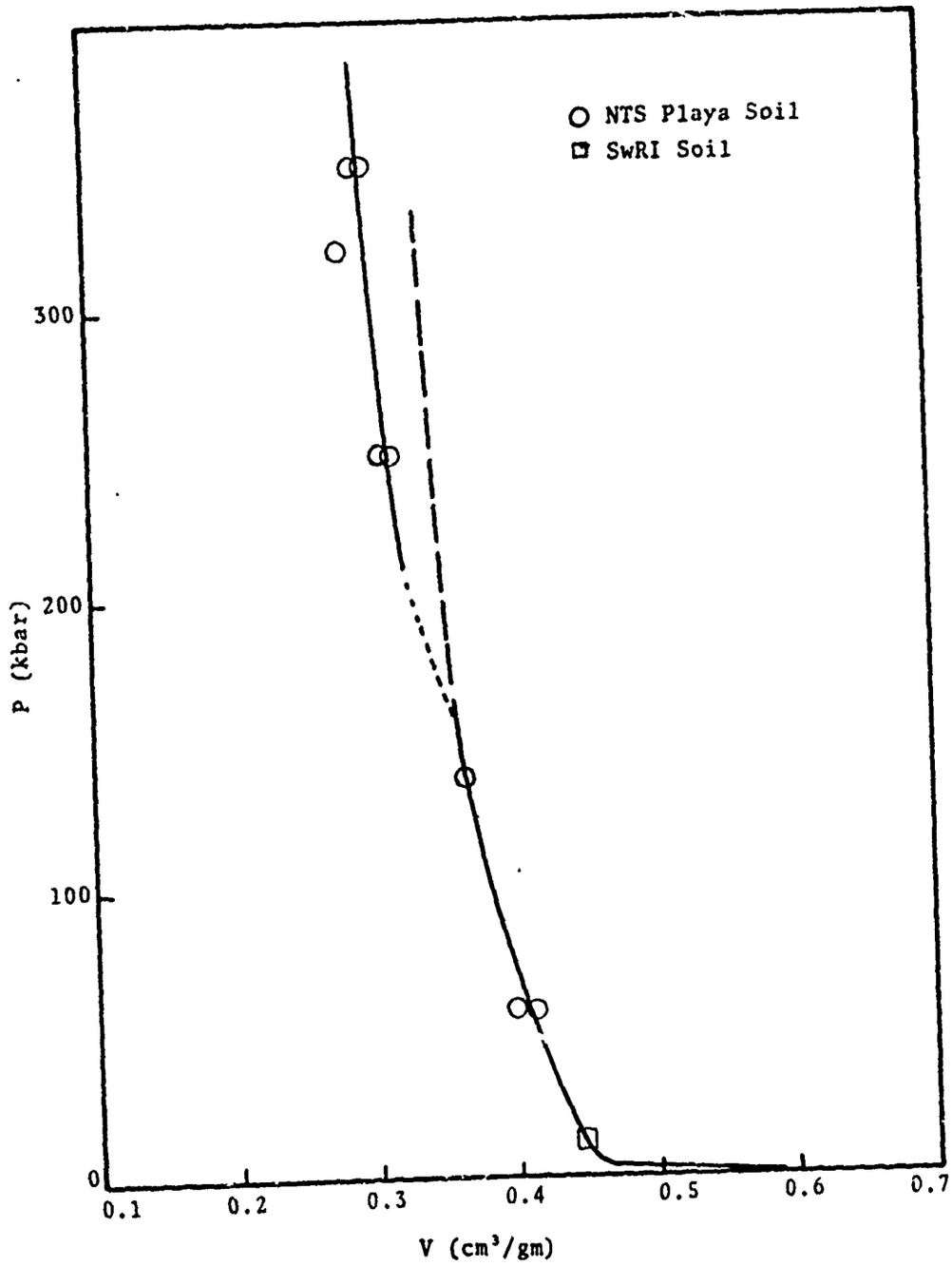

Fig. 6--Proposed revision of the equation of state of NTS playa soil.

McCormick Ranch sand, although the limited data match better the behavior of pure quartz.

- In incompletely saturated SwRI soil (ρ_0 = 1.36 gm/cm^3, w = 8.5 percent dry weight) complete collapse of pore volume occurs at stresses between 4 and 7 kbar.

In order to achieve a more complete understanding of the behavior of the properties of soils in the stress range of interest to explosive-soil interactions we make the following recommendations:

- A better gauge technique than used here is required for equation of state studies especially in dry soils. In-material magnetic particle velocity gauges offer the best hope for success.
- Measurements on dense (ρ_0 = 2.12 gm/cm^3) McCormick Ranch sand at about 15 kbar and between 50 and 100 kbar are needed to determine the curvature of the pressure volume relationship of the solids.
- Measurements of the equation of state of SwRI soil at high stresses would be helpful in determining the equivalence (or lack thereof) between SwRI soil and McCormick Ranch sand.
- Measurements of the equations of state of both soils at stresses below 7 kbar would be required to determine the details of pore collapse. To date no theoretical model is available to predict this behavior in soils. Such a model would aid immensely the understanding of low pressure soil behavior.

III. TEST PROGRAM

This work is an outgrowth of an earlier investigation of the effects of buried high explosive charges on steel plates conducted for MERDC by the Southwest Research Institute (SwRI) (Wenzel and Esparza[6]). In order to improve the capability to predict effects of land mines on vehicles, a computer code simulating the explosive-soil-target interactions has been developed. As part of this latter effort, a series of twelve model experiments were performed using precisely characterized soils to provide data as a check on the computed results. There were two main reasons for this approach: (1) there was considerable variation in the properties of the soil used by SwRI, and (2) there was no dynamic equation-of-state data for the SwRI soil so that the computer model used McCormick Ranch Sand, an entirely different soil. McCormick Ranch Sand was used in all of the present model experiments.

3.1 BACKGROUND

The SwRI report has been a major influence in this work and, consequently, the primary thrust of this background section will be directed toward that report. The brief summary of earlier work is based on the discussion of Wenzel and Esparza.[6]

3.1.1 Experiments with Unburied Explosive Charges

The earliest systematic investigations of the effects of explosive charges on vehicles are reported in several BRL reports (Hoffman and Mills[14]; Goodman[15]; Jack and Armendt[16]). These investigators measured pressure and impulse imparted to metal plates separated from explosive

charges by air or partial vacuum. These data were used by Cockrell, et al.[17] and Wenzel, et al.[18] to estimate survivability and vulnerability of tanks to land mines.

The loading of a metal plate from an explosive charge in air is accomplished by two means. First, a large amplitude, short-duration pulse is produced by a shock wave travelling through the air. This initial loading contributes very little impulse to the plate because of its short duration. The main portion of the total impulse to the plate is delivered by the expanding detonation products in a somewhat lower pressure but much longer duration pressure pulse. Jack and Armendt[16] have observed that the initial sharp peak is virtually absent in experiments at partial vacuum.

3.1.2 Experiments with Buried Explosive Charges

The effects of burial on blast effects was first investigated by Kincheloe.[19] Comparing his results with Goodman's[15], he concluded that buried charges are more efficient than charges in air, and that the impulse delivered is dependent on charge mass, separation distance and depth of burial.

Wenzel and Esparza[6] conducted an extensive and systematic investigation of the "pressures and impulses at close distances from explosive charges, buried and in air." They investigated both spherical charges and pancake charges with a diameter to thickness ratio of 3.16. They also conducted a small number of experiments with cylindrical charges in air. Their charges varied from 0.057 kg (0.125 lb) to 0.68 kg (1.5 lb), and they used standoff distances from 0.12 m/kg$^{1/3}$ (0.3 ft/lb$^{1/3}$) to 0.40 m/kg$^{1/3}$ (1.0 ft/lb$^{1/3}$).

The SwRI investigators measured impulse by the BRL plug technique. Pressures were measured by a Hopkinson bar technique in which high strength steel rods [nominal yield at 24 kbar (350 ksi)] were inserted into holes drilled through thick steel plates. The rods were separated from the plates by sleeves of silicone rubber. The pressure history of the end of a rod was transmitted up the rod and measured by a strain gauge on the surface of the rod. The stress-strain relation of the rod then permits conversion of strain to stress. This relation was determined both statically and dynamically, although it is not clear from their report if the calibration extended over the entire range of observations.

Briefly summarized, their results on buried explosives were:

- Peak stress falls off more rapidly away from the axis of the experiment for pancake charges than for spherical ones.
- There was little, if any, observed effect of scaled depth of burial for scaled depths of 2 and 4 inches (5 and 10 cm). For a scaled depth of 10 inches (25 cm) there was an increase in peak stress.
- Axial pressures produced by pancake charges averaged 2.5 times those produced by spheres.
- Buried spherical charges delivered considerably greater peak stress than corresponding charge in air. However, for the pancake charges there was little apparent difference.
- Water content of the soil has a significant effect on the pressure delivered to the plate, with wetter soils producing higher pressures.

3.1.3 Systematics in the SwRI Data

In the initial stages of the present work we conducted a detailed re-examination of the SwRI report just described. The goal of this effort was to identify any weaknesses in their techniques in order to improve the quality of our own experiments. In the course of this re-examination we have discovered some systematic effects apparently overlooked in that report.

Wenzel and Esparza tabulate the soil water content and bulk density for all their buried experiments except for two shots in "mud." These data are plotted in Figure 7. In a plot of this nature it is readily apparent that the soils used fall predominantly into one of two groups. The larger of these two groups has water content (w) between 5.1% and 11% of dry soil weight and density (ρ) from 1.18 gm/cm^3 to 1.51 gm/cm^3 with a mean of w= 8.4% and ρ= 1.36 gm/cm^3. A smaller, more compact group centered at w = 3.4% and ρ= 1.53 gm/cm^3 has 2.5%< w< 4.5% and 2.48 gm/cm^3<ρ< 2.62 gm/cm^3. The large scatter of soil states is undoubtedly due to lack of control of water content and density of the soil directly. The SwRI workers compacted all soils by a similar process but soils of different water contents will respond to that process differently.

The wide variability of soil conditions studied by SwRI permits investigation of the effects of soil properties on blast effects. Let us restrict our discussion to soils falling into either of the two groups described above and reject other soils as "anomalous." If we then plot the ratio of observed peak stress, P_b, to the peak stress for the same charge at the same distance in air, P_a, as a function of soil density we find a definite positive correlation for spherical charges (Figure 8a) but no apparent correlation for pancake charges (Figure 8b). So we may ascribe some of the scatter of the SwRI data to variations of density.

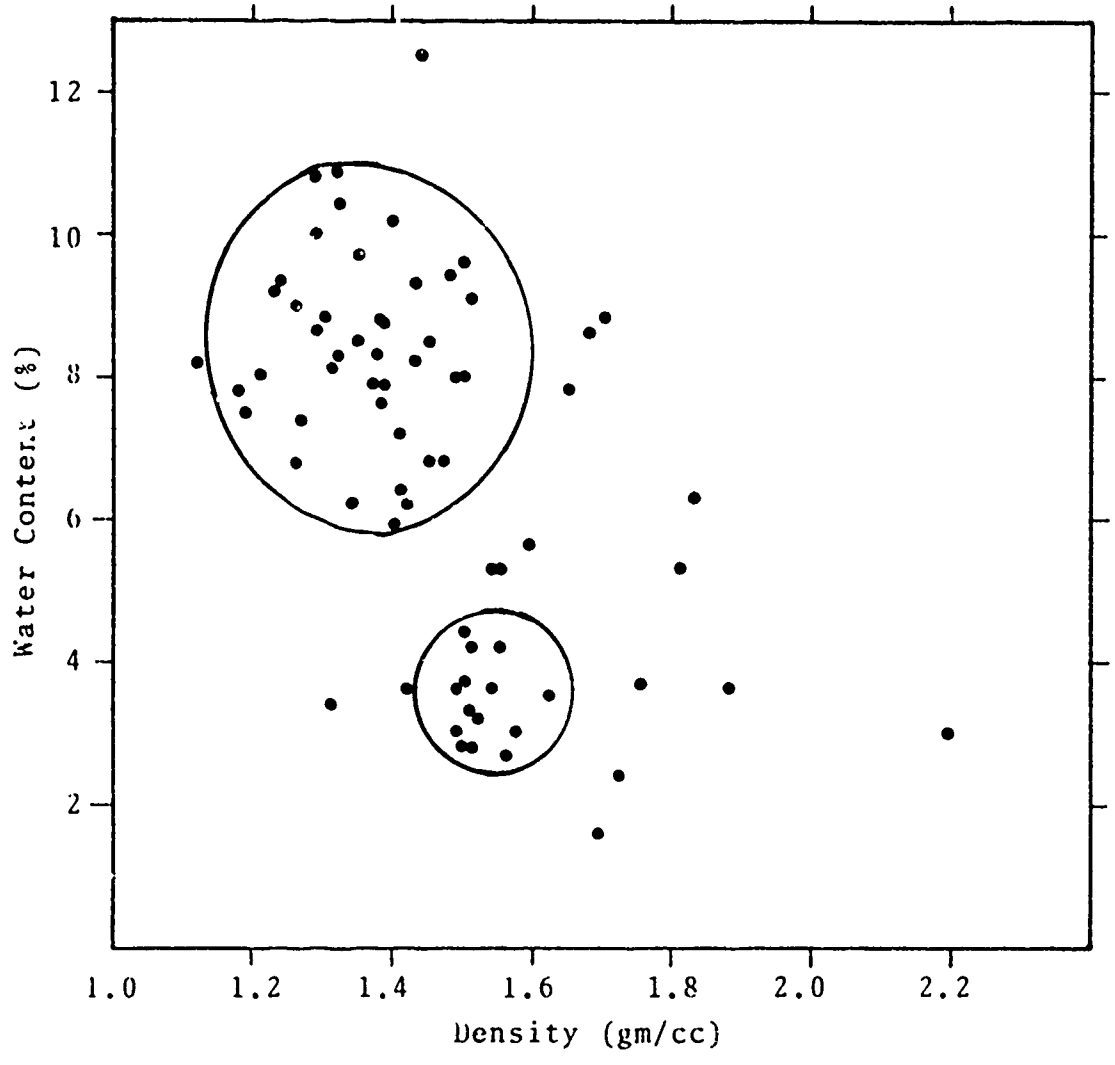

Figure 7. Water content plotted versus density for the soils used in the experiments reported by Wenzel and Esparza[6]. "Wet" and "dry" groups are encircled.

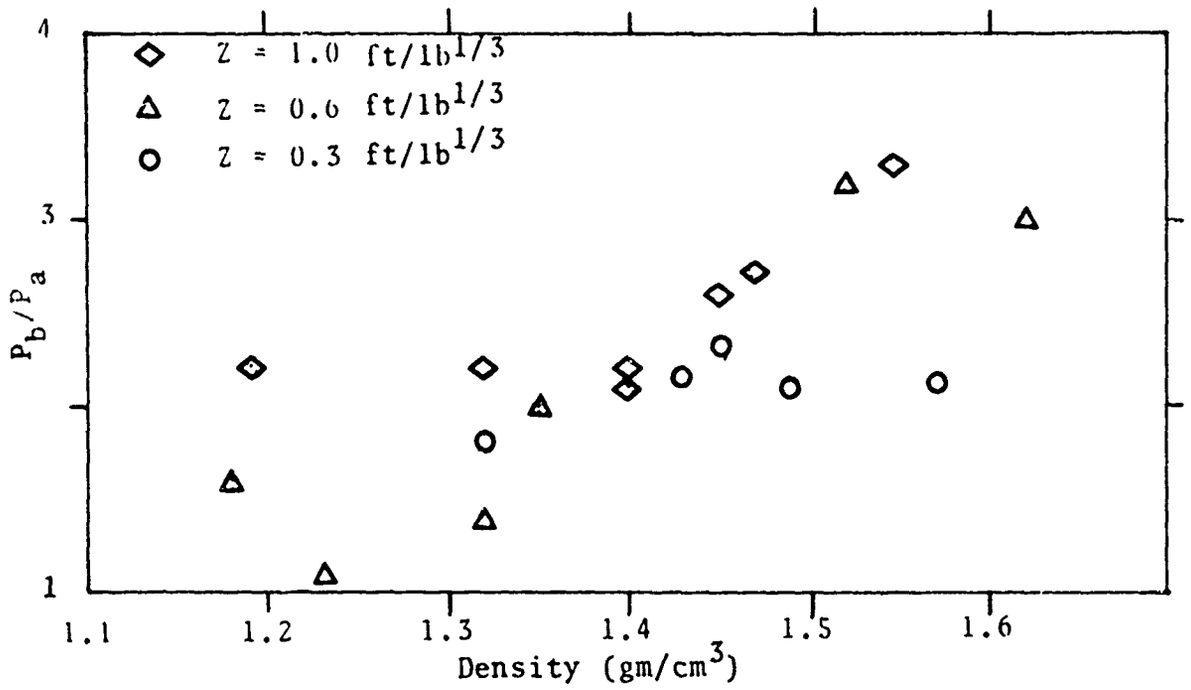

Figure 8a. Normalized pressure-density relation for buried explosive spheres.

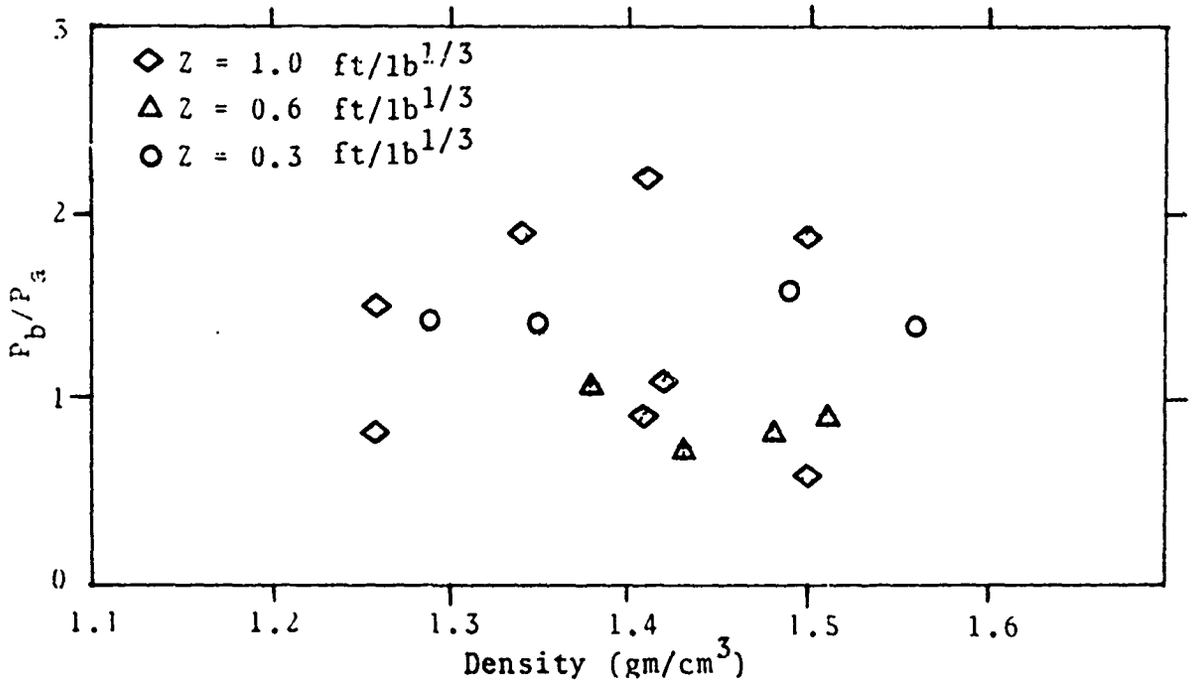

Figure 8b. Normalized pressure-density relation for buried explosive pancake charges.

Next, we note that for nine of their soil conditions Wenzel and Esparza determined the sound speed. Four of these cases were for spherical charges where peak stress on axis was also measured. In these cases we can calculate the acoustic impedance $Z_o = \rho_o c_o$. If the normalized peak pressure (on axis) is plotted against the impedance we see an even stronger positive correlation (Figure 9). It seems likely, therefore, that much of the scatter in Figures 8a and 8b may be due to variations in the sound speed of the soil. Based on the scaling relations of Wenzel and Esparza, this result is not at all unexpected.

It is interesting to note that the actual depth of burial seems to be more closely related to measured peak stress than the scaled depth of burial. Figure 10a is a plot of real depth of burial versus the normalized pressure for spherical charges. There is a weak, but nonetheless distinguishable, effect of real depths of burial on the peak pressure as indicated by the dashed line in the figure. When scaled depth of burial is used as the abscissa as in Figure 10b no systematic relation can be seen. We conclude, therefore, that peak pressure is more closely related to real depth of burial than to scaled depth of burial for soils.

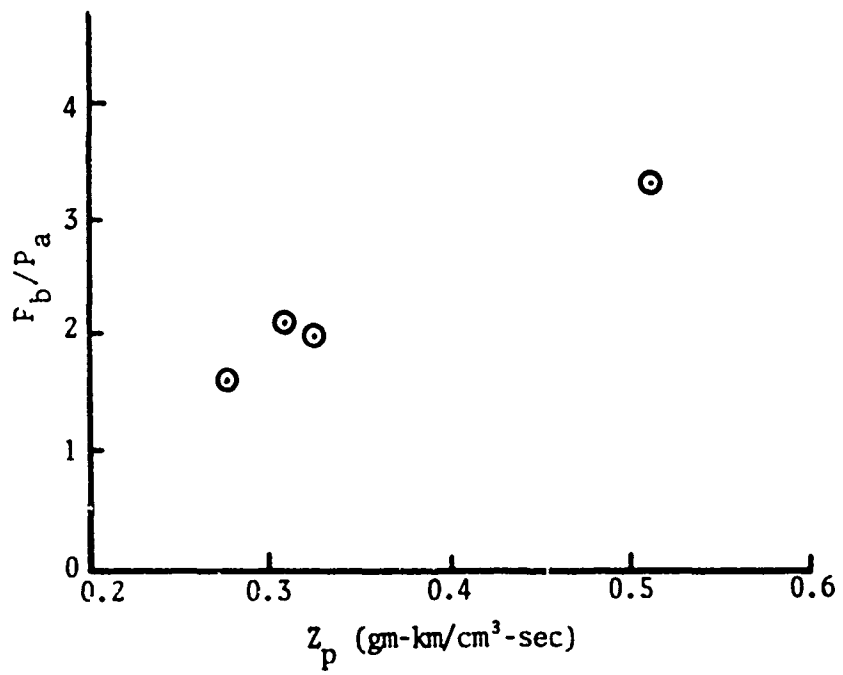

Figure 9. Normalized peak pressure plotted versus impedance for various soil conditions used in the experiments conducted by Wenzel and Esparza[6].

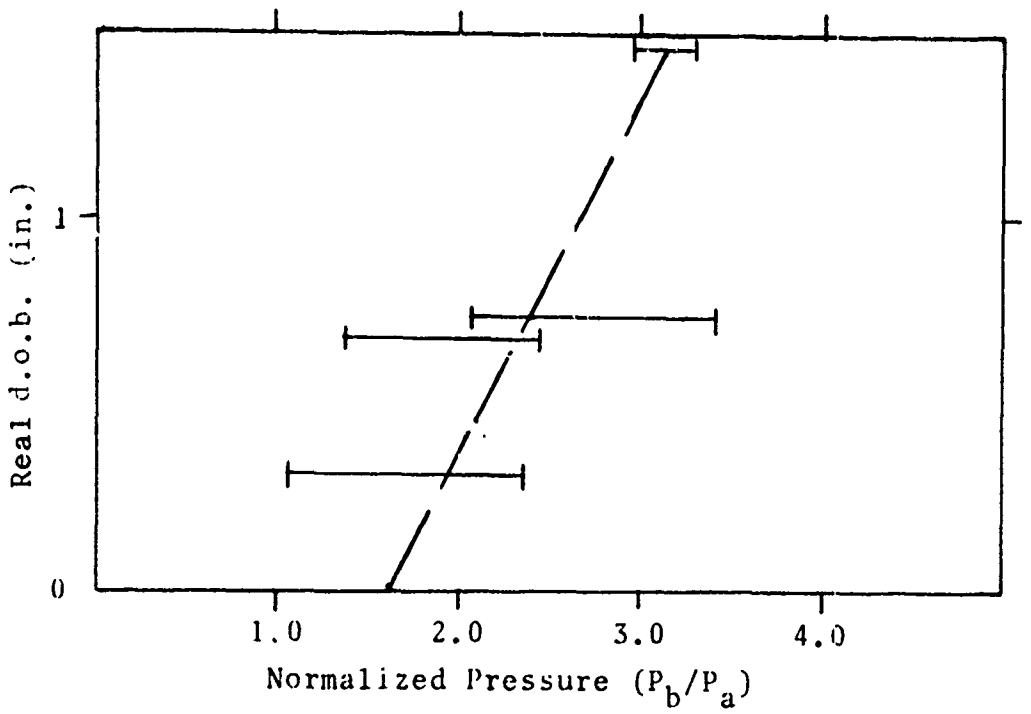

Figure 10a. Plot of real depth of burial versus normalized pressure for spherical charges. Dashed line indicates trend of data.

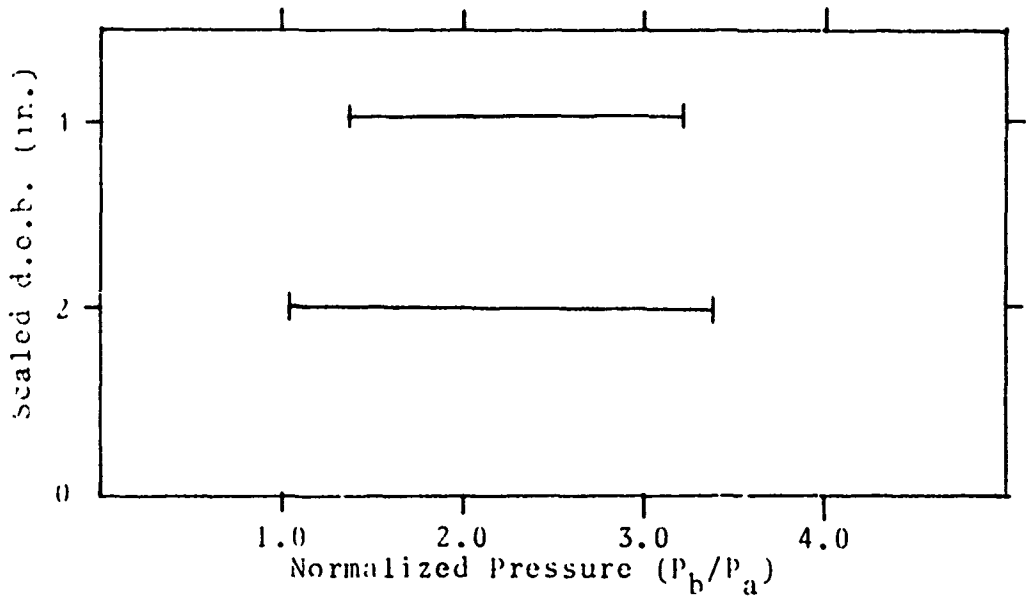

Figure 10b. Plot of scaled depth of burial versus normalized pressure for spherical charges.

3.2 APPROACH

3.2.1 General Experiment Plan

In the current effort twelve experiments have been conducted with buried high explosive charges--two charge configurations were used, spherical and 3:1 (diameter: thickness) pancake, and two different soil conditions were used. Three experiments were done for each combination of charge and soil. In all of the experiments the charge was buried under 2.54 cm (1.00 inch) of the test soil. Stress histories were measured in a mild steel plate suspended over the soil so its bottom surface was at a scaled height of 0.13 $m/kg^{1/3}$ (0.3 $ft/lb^{1/3}$). A cross-section of the test set-up is shown in Figure 11 for both configurations.

The explosive used in these experiments was C-4. The initial plan had been to use 1.15 kg (2-1/2 pounds) for each charge whether spherical or pancake. However, a 10.3 cm (4-1/16 inch) diameter spherical mold which held 0.95 kg (2.1 lb) of C-4 was already available, so it was decided to take advantage of scaling relations and use the smaller charge.

3.2.2 Soil Preparation

The main purpose of these experiments was to provide experimental data with which to check the computer modelling of buried charges described previously. Consequently, it was of utmost importance that the soil used be well characterized. The soil chosen was McCormick Ranch sand from near Albuquerque, New Mexico. This soil has been investigated in both static tests (Mazanti and Holland [4]) and dynamic tests (Peterson and Gates [5]). Since only a limited amount of soil was

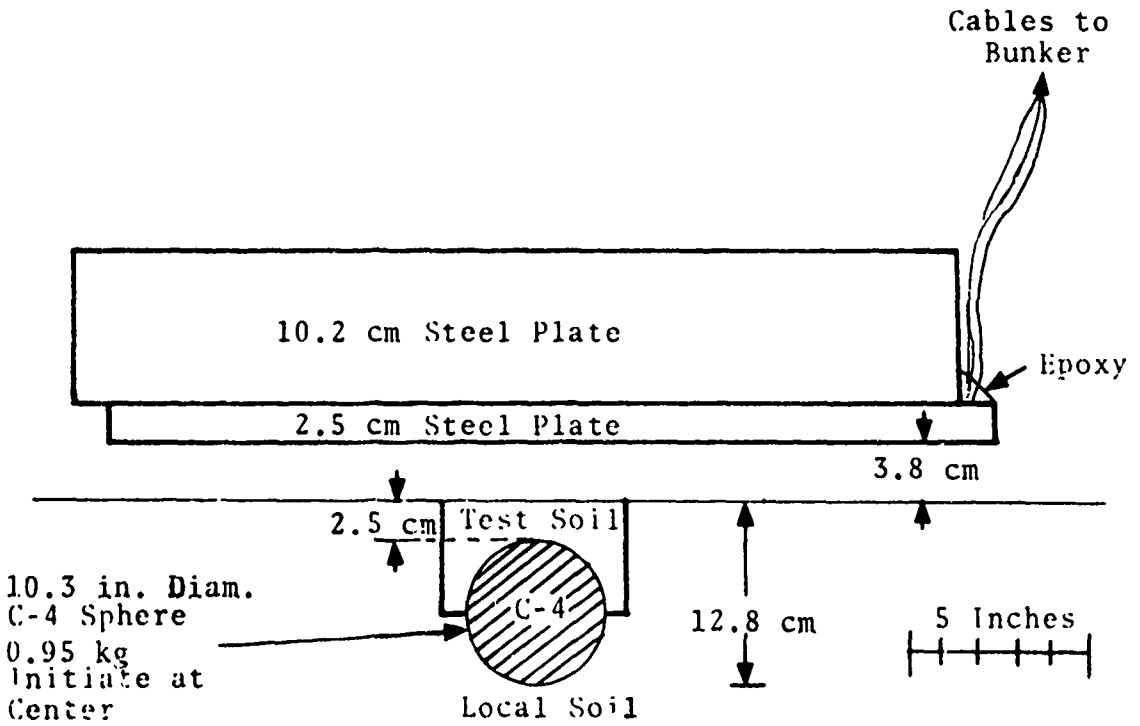

Figure 11a. Cross-section of experimental arrangement for buried explosive spheres.

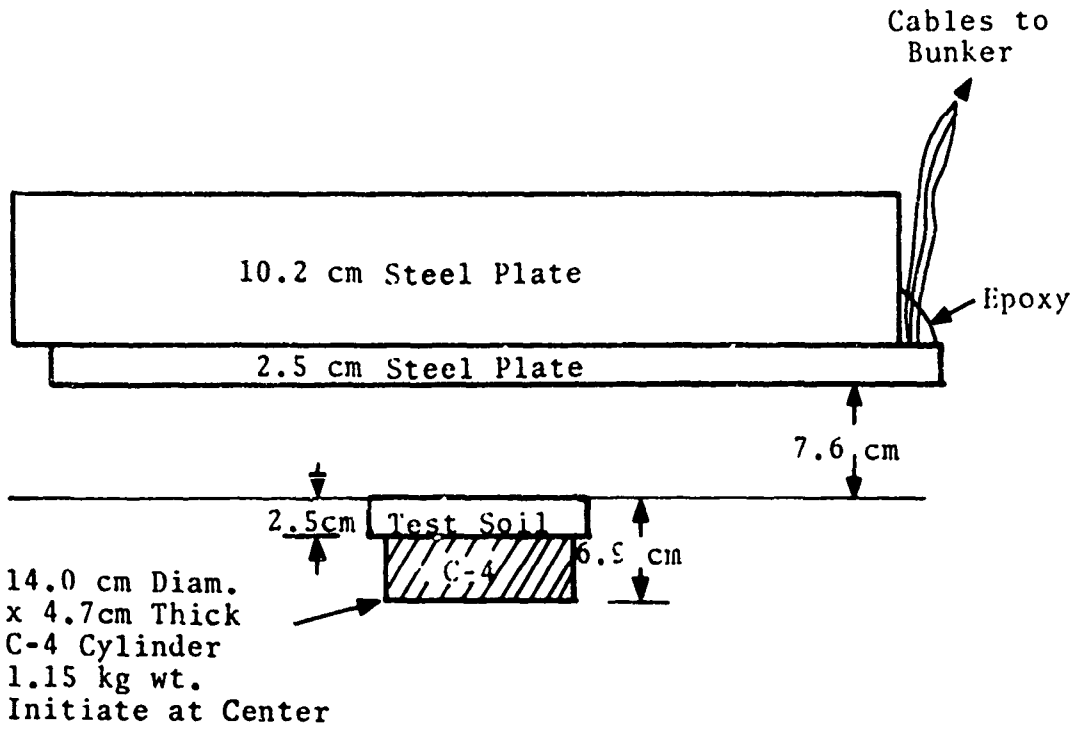

Figure 11b. Cross-section of experimental arrangement for buried explosive discs.

available to us (Stanford Research Institute (SRI) supplied us with about 40 kg of soil), it was decided to use the test soil only above and around the spherical charges and only above the pancake charges. This decision involved the trade-off between having a homogeneous soil throughout the test bed and having a very precisely known soil where it should have the greatest effect. Clearly, we have considered the latter to be the more important.

The natural soil at the Green Farm Test Site is very rocky, so enough soil was sifted through a 3-mm (1/8-inch) screen to conduct our tests. Since this rather tedious procedure had to be resorted to, it was decided to perform the entire test in a "sand box" 0.9 m x 0.9 m x 0.3 m (3 feet square by 1 foot high). These dimensions are sufficient that edge effects were unimportant during the period of taking data. This procedure considerably shortened the process of setting up the experiment.

The two soil conditions studied were density ρ = 1.36 gm/cm^3 and water content w = 8.5% of dry weight, and ρ = 2.12 gm/cm^3 and w = 12% of dry weight. The former is already familiar to the reader as the mean of the larger of the two groups of soil conditions studied by Wenzel and Esparza.[6] It is also rather close to the *in situ* water content of the local soil in late summer (7.5% of dry weight). We chose this soil condition with the hope that our results could be compared directly to those of the earlier study. The latter soil condition is that used by Peterson and Gates[5] in their low velocity gas gun experiments. It is near the state studied by Mazanti and Holland[4] who used ρ = 1.87 gm/cm^3 and w = 11.4% of dry weight.

Soil was received in three batches, two for the final experiment only. The first batch as received from SRI had a water content of 8.4%. The entire volume of soil was sifted through a 1-mm sieve to eliminate the few small pebbles present. This material was used for both the equation-of-state studies described previously and the present experiments. For the drier soil condition this sifted soil was used directly, whereas water was added for the wetter condition to bring the water content to 12%. An appropriate mass of soil was then loaded into a mold of a shape to conform with the charge, and compressed to the proper density. The wet soil, which was cohesive, was then removed from the mold and placed in a plastic bag to prevent water loss. The dry soil, which was not cohesive, was retained in the mold until buried when the surrounding soil would support it.

3.2.3 Measurement Techniques

In all of the experiments, stress histories were measured at various locations within the steel plate using manganin piezoresistive gauges. Initially, an attempt was made to measure the velocity of the upper surface of the plate by a Moiré technique. These attempts were not successful because of the low velocity of the plate but are summarized below, since the technique would be useful for situations for which the rear free surface velocity of the plate were higher. In the final ten experiments the surface velocity was measured by shorting pins above the top of the plate over the center of the charge.

3.2.3.1 Manganin Gauges

Stresses within the steel plates were measured by manganin gauges. This technique was chosen for several reasons. First, because of the high density of the soil in some of our experiments

we expected peak stresses to exceed the yield strength of any available steel. This eliminated the use of a Hopkinson's bar technique such as that used by Wenzel and Esparza (1972). Second, our personnel have considerable experience in both the use and calibration of these gauges. Finally, even though there are some non-linearities at low stresses (below 30 kbar) and considerable hysteresis on unloading, both these conditions have been sufficiently studied so as not to hinder interpretation of the records.

In order to emplace the gauges within the steel plates each plate was made up of a stack of two or more plates with gauges between the plates. The gauges were first glued to the lower plate with C-7 epoxy and, after that epoxy had cured, the entire joint between plates was filled with C-7. This epoxy layer was about 0.4 mm (0.015 in.) thick. Two gauge layouts were used. In the majority of experiments a two-layer plate was used with all the gauges located as in Figure 12 in the same plane. We refer to this layout later as H (horizontal). In one of these experiments (2144) the lower plate was 5 cm thick. In three experiments (one for each configuration except a spherical charge buried in dry soil) the plate consisted of five plates with a gauge at each joint on the axis of the charge (see Figure 13). These experiments were conducted to determine the amount of attenuation of the peak stress as the pulse traveled through the steel plate. We refer to this later as the V (vertical) layout.

The gauges used were Pulsar FM50A gauges. These gauges are mounted between fiberglass and kapton. The gauge itself is only about 0.002 cm thick but the entire package thickness is controlled by internal solder joints and is about 0.4 mm (15 mils) thick. The gauges were used in a two-lead arrangement and were powered by a Pulsar Model 251A which also contains

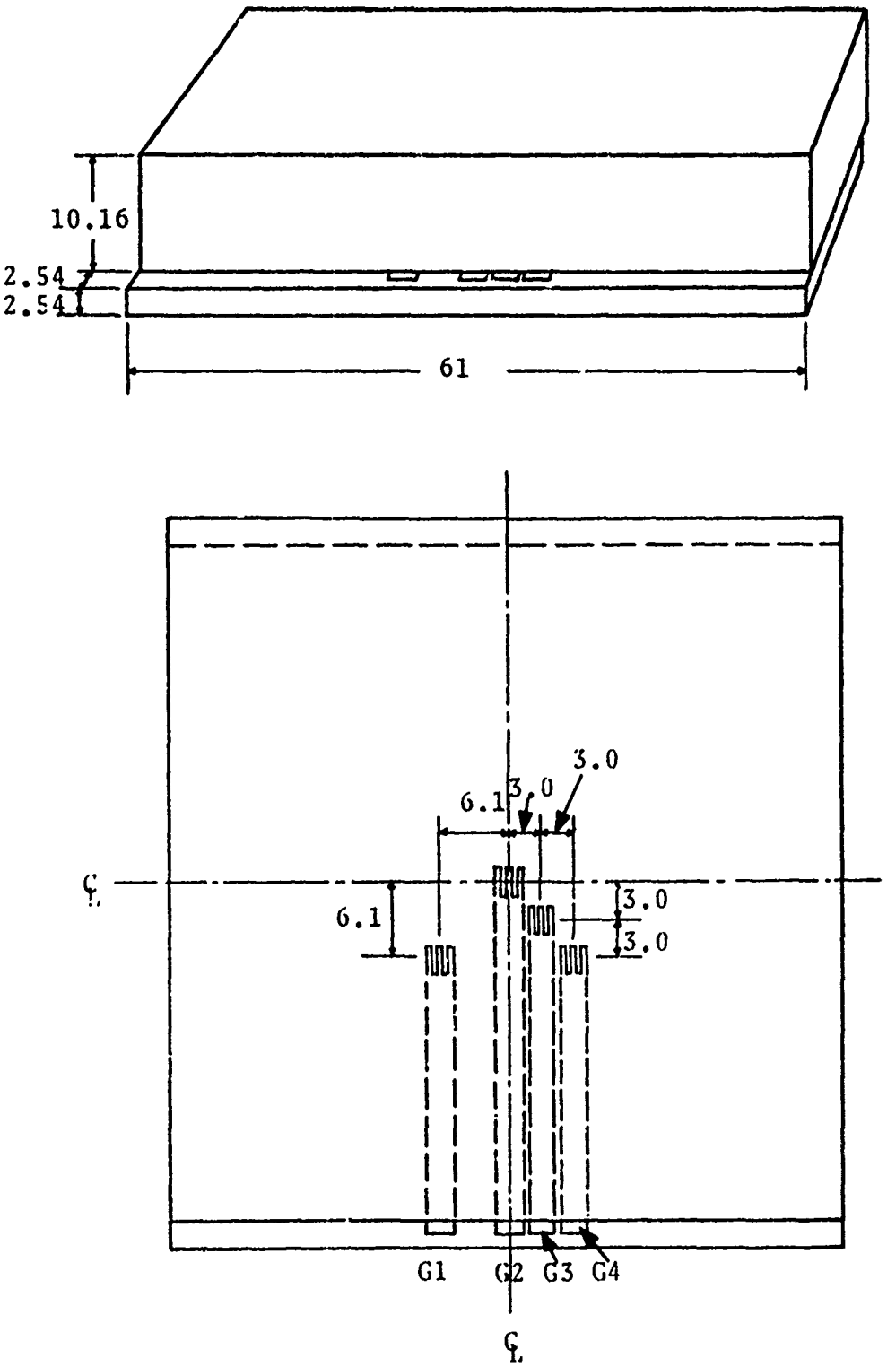

Figure 12. Gauge layout for "II" configuration. All dimensions in centimeters.

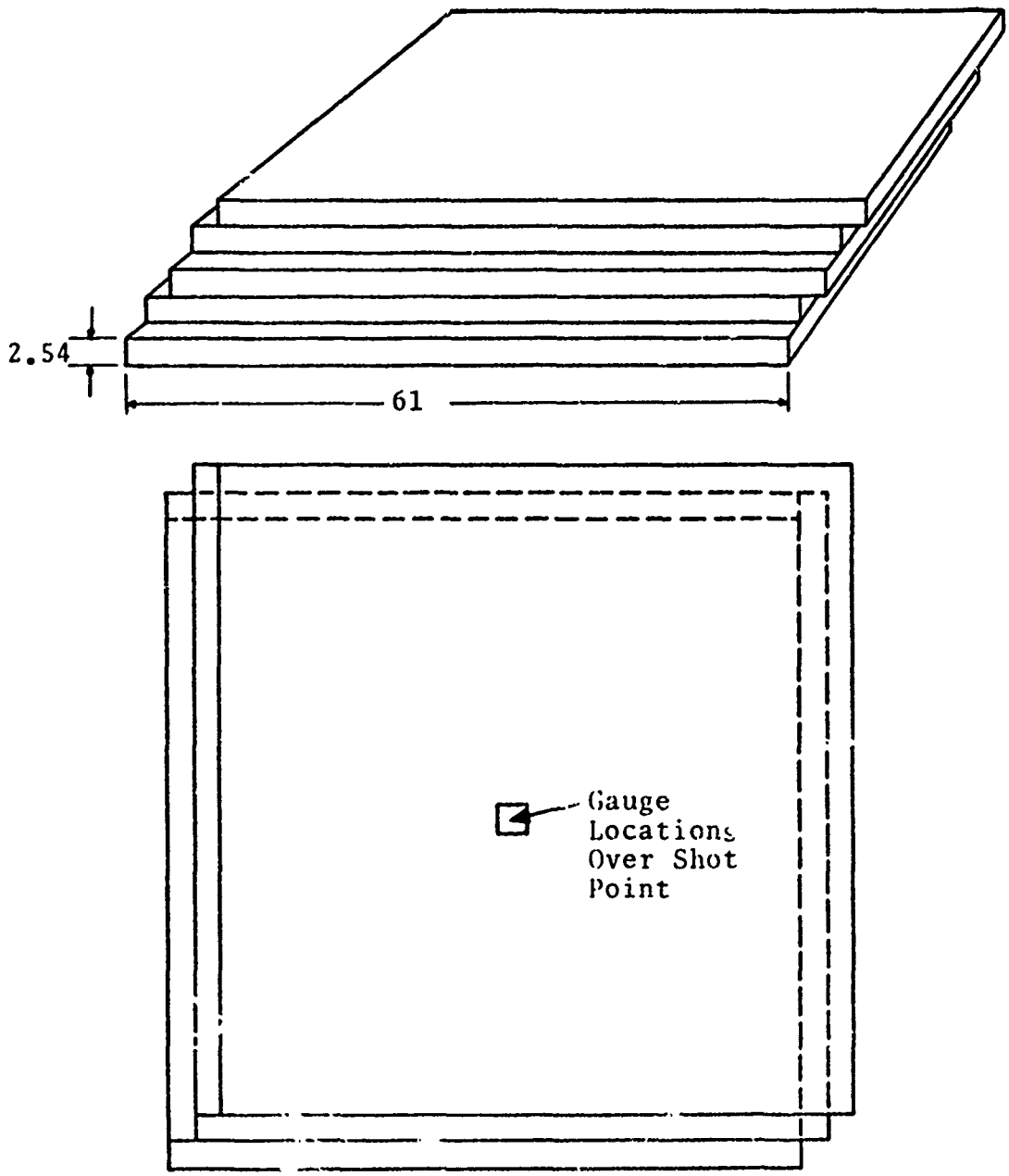

Figure 13. Gauge layout for "V" configuration.

the bridge circuit to convert changes in gauge resistance to changes in voltage. Prior to each shot the circuits were calibrated by putting a known resistance in series with the gauge.

3.2.3.2 Moiré Fringe Measurements of Surface Velocity

Use of Moiré fringes is a standard technique for the measurement of strain in "static" tests. We give a very brief discussion of the general technique here and refer the reader interested in details to the literature (e.g., Dove and Adams[20]). When two grids are superimposed, a new pattern of alternating light and dark bands can be seen. This effect, known as the Moiré effect, is caused by overlapping of positive and negative features of the two grids. If one of the grids is deformed the "fringes" show the deformation. It is the mechanical analog of optical interference phenomena. Such an effect can also be produced by superposition of a screen and its shadow.

We had hoped to use this technique to measure the motion of the upper surface of the plate in our experiments. Initial feasibility experiments showed that the method was a good one in principle. A 1/2-in.-thick, 12-in.-square steel plate was placed on top of a 1/2-pound sphere of C-4. The upper surface of the plate had a grid of 1/8-in. lines on 1/4-in. centers. This setup was viewed with a high-speed framing camera through a similar grid. The resulting pictures, obtained when the charge was detonated, show very clearly the deformation of the steel plate. The results of this experiment are given in Figure 14. Note that the surface velocity in this case is about 170 m/sec.

In our first two buried charge experiments, we attempted to use this same technique to measure the surface velocity.

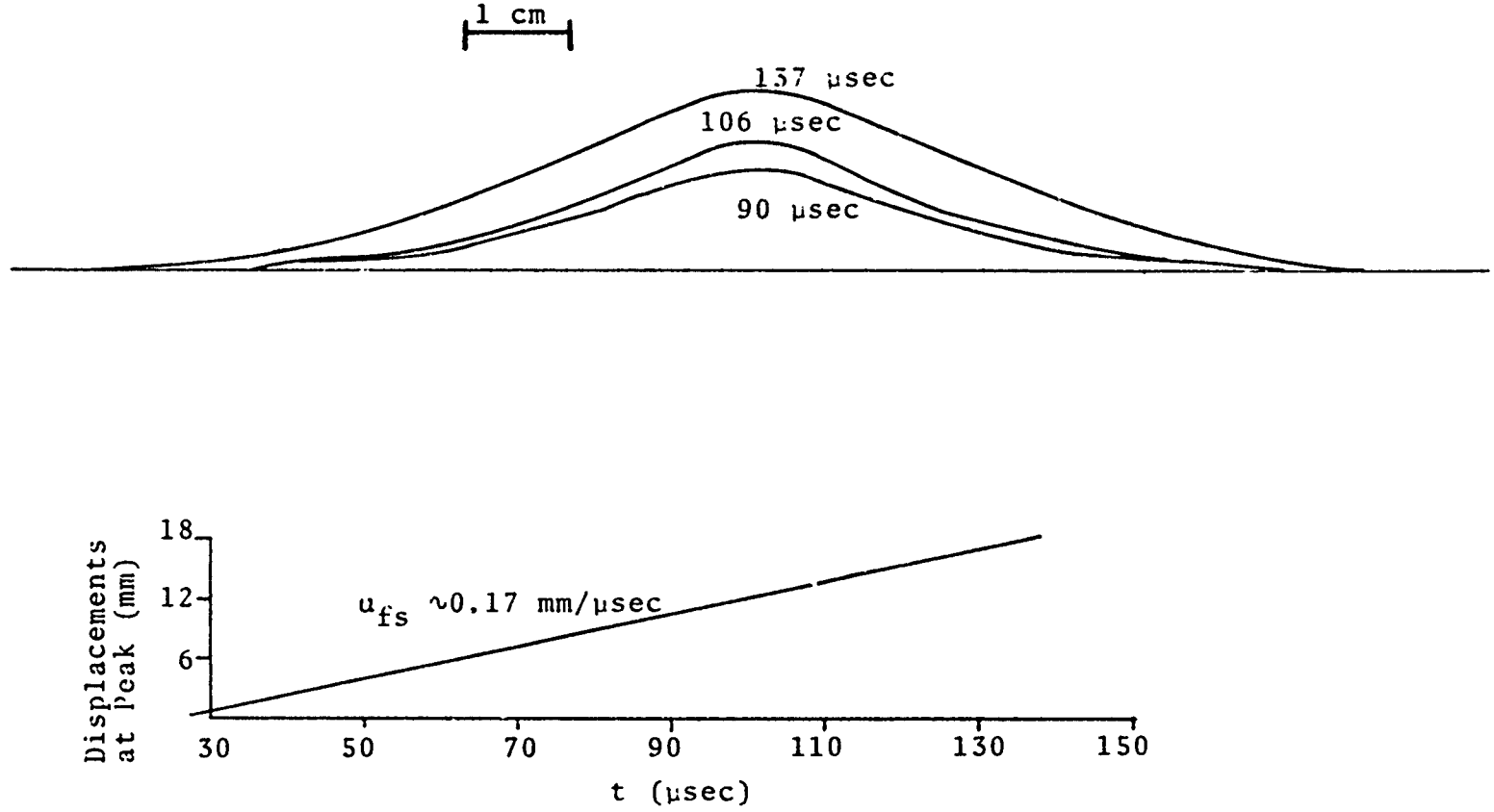

Figure 14. Surface profiles derived from Moire fringe data and peak-free surface velocity determinations.

The optical arrangement is shown in Figure 15. The grid on the steel surface was illuminated by an explosive argon candle not shown in the figure. The experiments did not provide any velocity data due to the low velocity of the surface. This was true even though the grid pitch was twice that used in the feasibility study. Later measurements using pins (Section 3.2.3.3) showed that the velocity was only 8 percent of the value obtained with the thin plate.

Although the Moiré fringe technique failed in these particular experiments, it is a promising technique for higher velocities and can be used to measure velocities over an entire surface.

3.2.3.3 Velocity Pin Measurements

In the final ten experiments the surface velocity was measured by means of charged pins which were shorted by contact with the steel plate. These pins, of soft copper, were held in a plexiglas retainer and supported just above the plate. The velocity was calculated by dividing the known spacing of the pins by the time lapse between shorting signals. In some cases, the velocity was not constant as the plate rose, but rather decreased with time. In these cases the first measured velocity is reported.

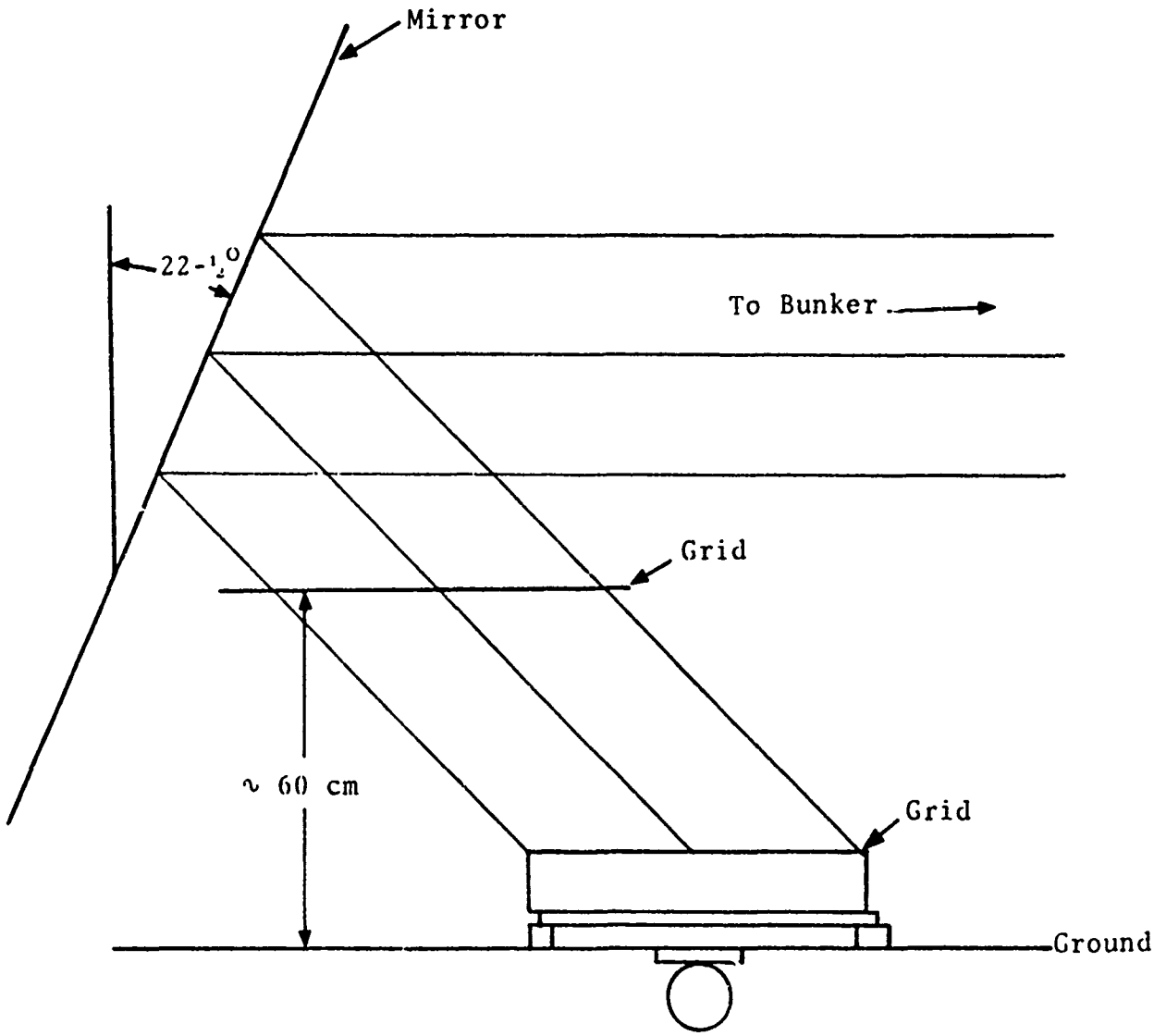

Figure 15. Optical arrangement for Moiré fringe experiments.

3.3 RESULTS

The data derived from these experiments are tabulated in Table IV. Figure 16 shows data for a typical H configuration and Figure 17 shows data for a typical V configuration. A telephoto picture of an experiment in progress is shown in Figure 18.

3.4 DISCUSSION

In this section we discuss the results of the experiments themselves and in relation to the work of Wenzel and Isparza.[6] Comparison of the experimental results with the computational model is deferred.

3.4.1 Effects of Nonplanar Stress Waves

The manganin foil stress gauge is designed to measure stress in a planar wave traveling normal to the gauge plane. The waves studied in this work do not perfectly meet the requirements of planarity and normality. This is especially true for gauges used to measure stress off the axis of the charge. However, the effects of these disparities are probably rather small in the present applications. Figure 19 is an example of the worst effects of nonplanarity. The oscillations prior to arrival of the main wave are due to the diverging nature of the wave. The records shown in Figures 16 and 17 are typical of almost all of the data.

3.4.2 Reproducibility

One of the principal goals of the present study was to achieve a high degree of reproducibility of our results by

TABLE IV

EXPERIMENTAL RESULTS: LAND MINE MODEL SHOTS

Shot No.	Soil		Shape	r(cm)[a]	R(cm)[b]	P_{max} (kbar)	V(m/s)	Δt(μs)[c]
	Water	Density						
2092	Dry	1.36	Sphere	0	14.1	23	--	16
				8.62	14.1	3.1		>20
2093	D	1.36	Sphere	4.31	14.1	9.8	--	80
				8.62	14.1	4.0		60
				8.62	14.1	3.5		--
2106	D	1.36	Sphere	0	14.1	19	13	45
				4.31	14.1	8.3		80
				8.62	14.1	4.1		65
				8.62	14.1	2.2		55
2115	Wet	2.12	Sphere	0	14.1	37	34	15(29)
				0	16.6	24		13(26)
				0	19.2	16		17(28)
				0	21.7	9.3		14(25)
2132	W	2.12	Sphere	0	14.1	35	18	12(24)
				4.31	14.1	10.6		13
2143	W	2.12	Sphere	0	14.1	36	15	17(32)
				4.31	14.1	21		13(27)
				8.62	14.1	8		50
				8.62	14.1	4		46
2138	W	2.12	Pancake	0	14.9	62	68	17
				4.31	14.9	36		13(32)
2139	W	2.12	Pancake	0	14.9	76	65	16
				0	17.4	52		17(20)
				0	20.0	36		20(24)
				0	22.5	27		12(16)
2144	W	2.12	Pancake	0	17.4	45→66[d]	42	16(20)
				4.31	17.4	29→42		16(20)
				8.62	17.4	11→16		16
				8.62	17.4	11→16		10(14)
2140	D	1.36	Pancake	0	14.9	69	21	17
				8.62	14.9	8.8		21
2150	D	1.36	Pancake	0	14.9	68	45	14
				4.31	14.9	37		>9
				8.62	14.9	10		34
				8.62	14.9	9.0		>12
2153	D	1.36	Pancake	0	14.9	64	50	18
				0	17.4	38		17
				0	20.0	25		22
				0	22.5	19		18

[a] Horizontal distance from charge center.

[b] Vertical distance from charge center.

[c] Time duration to first stress minimum. Value in parentheses () includes any "precursor" or ramp (see Figure 16, Scope B2).

[d] → indicates value projected to 2.5cm from lower surface of plate.

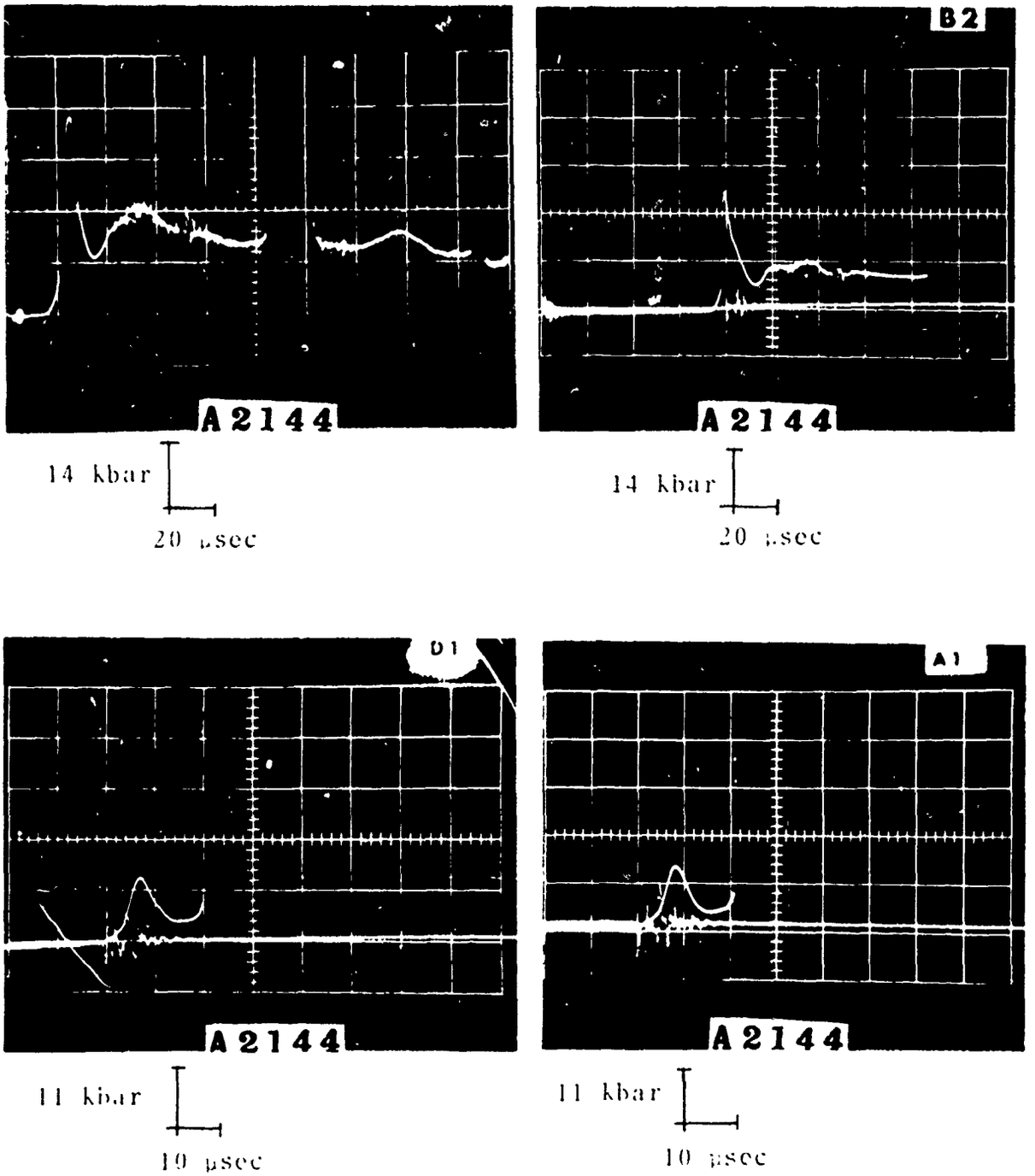

Figure 16. Manganin gauge record for an H configuration with wet soil and a pancake charge. Gauges 1 and 4 (scopes D1 and A1) survived longer with spherical charges than with pancake charges.

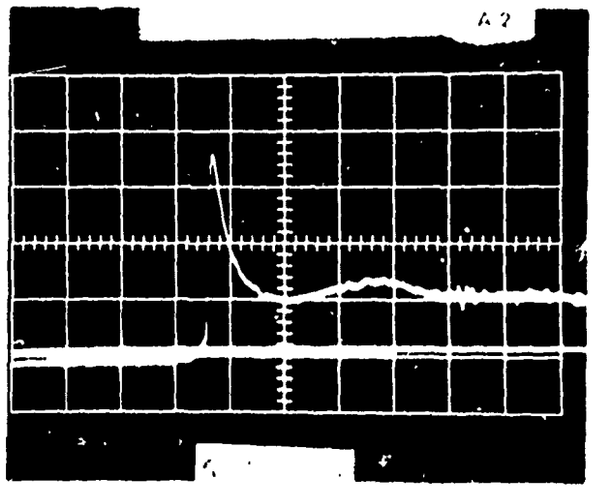

17(a) Manganin gauge record at r = 0, R = 14.9 cm; Peak Stress 64 kbar. Horizontal Scale 10 μsec/div. Vertical Scale ∿ 17 kbar/div.

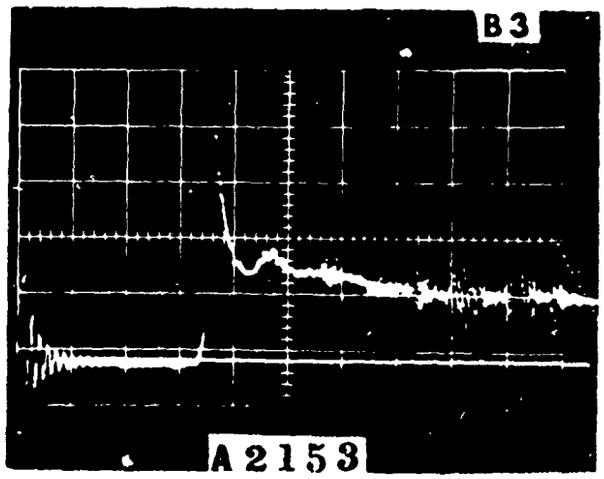

17(b) Manganin gauge record at r = 0, R = 17.4 cm; Peak Stress 38 kbar. Horizontal Scale 20 μsec/div. Vertical Scale ∿ 7 kbar/div.

Figure 17. Representative experimental data from a V configuration shot with a pancake soil in dry sand.

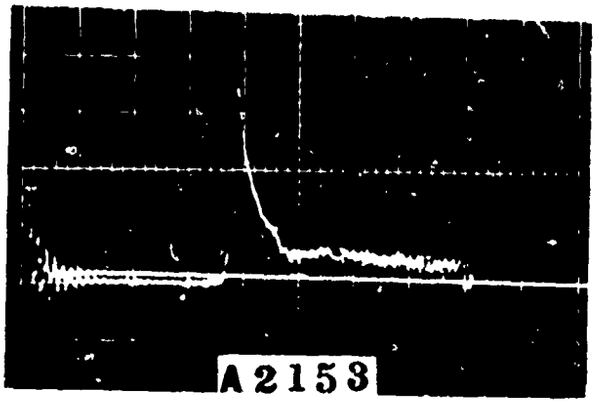

17(c) Manganin gauge record at r = 0, R = 20.0 cm; Peak Stress 25 kbar. Horizontal Scale 20 μsec/div. Vertical Scale ~ 7 kbar/div.

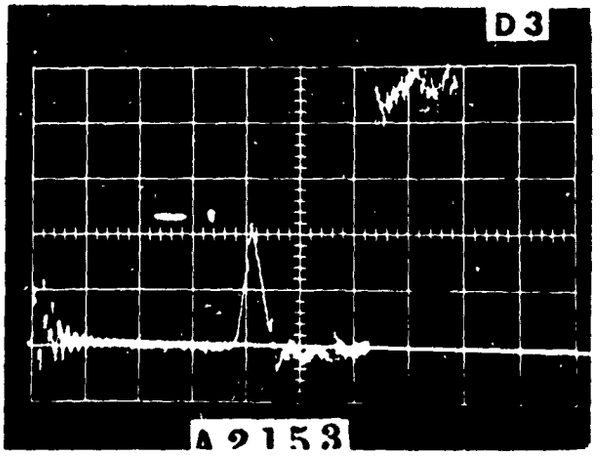

17(d) Manganin gauge record at r = 0, R = 22.5 cm; Peak Stress 25 kbar. Horizontal Scale 20 μsec/div. Vertical Scale ~ 9 kbar/div.

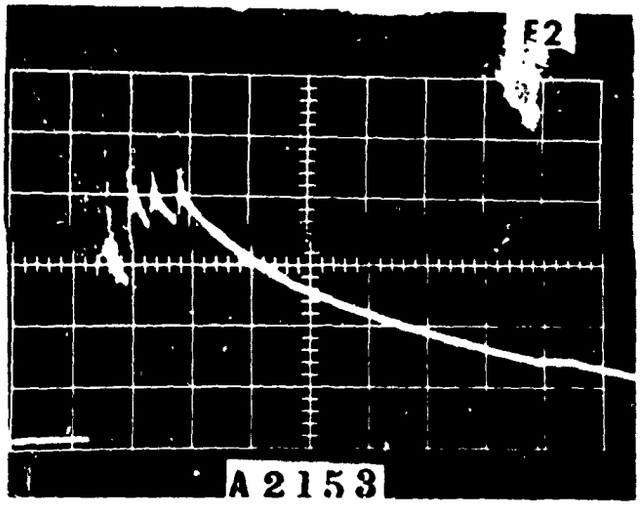

17(e) Velocity pin record with free-surface velocity of ~ 50m/sec. Pin spacing ~ 0.025 cm; Horizontal Scale 10 μsec/div.

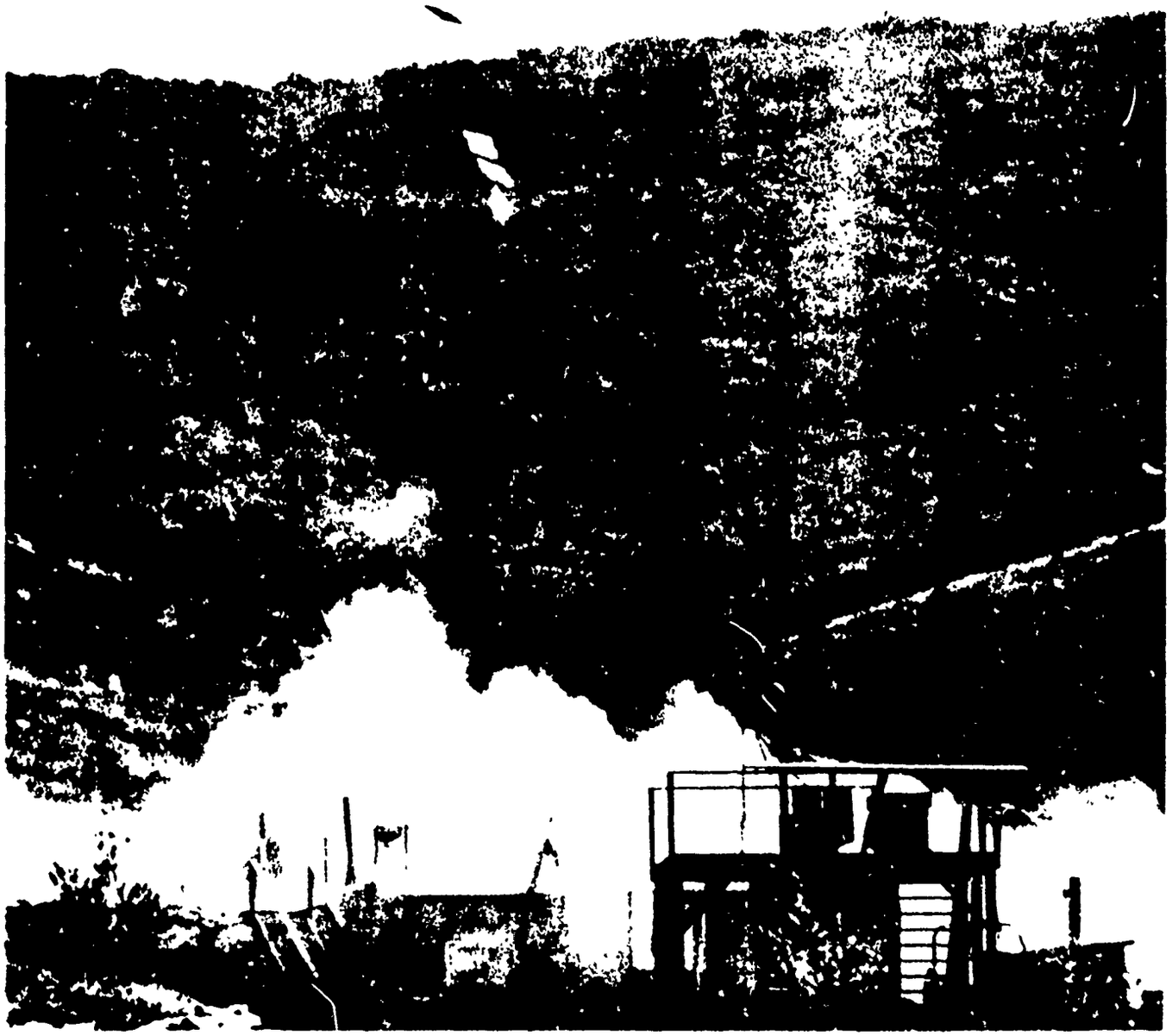

Figure 18. Shot Number A2115, a typical V configuration experiment.

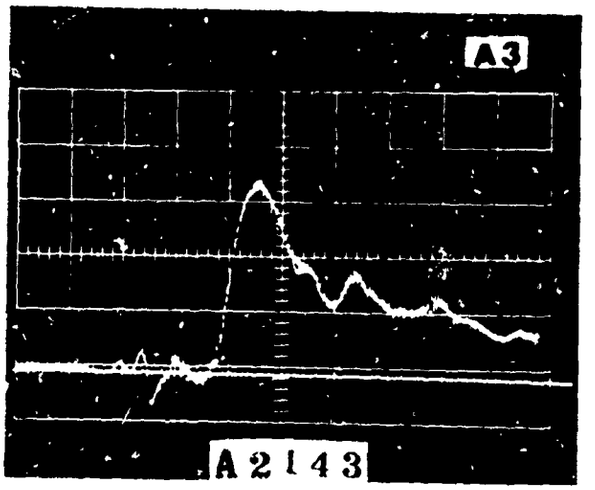

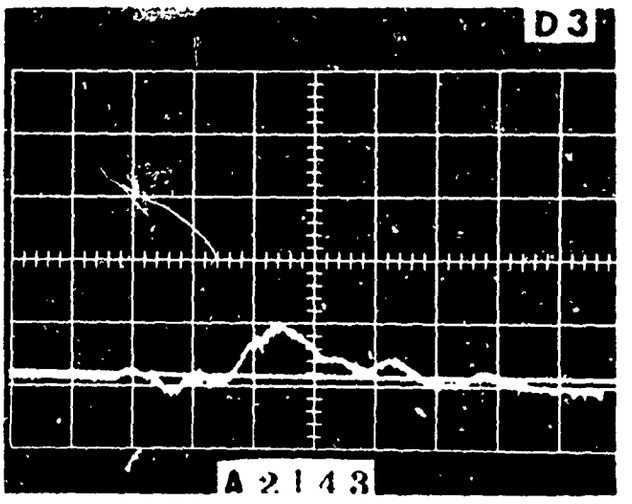

Figure 19. Typical "worst" result showing effects of nonplanar wave fronts on manganin gauge records. These records were taken with r/R = 0.61, using a spherical charge buried under one inch of wet soil.

careful soil preparation techniques. This proved to be somewhat difficult for experiments with spherical charges buried in dry soil, primarily because of the difficulty of preparing dry soil packed around spheres. Even in this case, peak stresses at similar locations were within 4 kbar of each other. Reproducibility in other cases was excellent. Figure 20 shows the on-axis stress histories for three different shots with a pancake buried under dry soil. Not only are the peak stresses within ± 4 percent, but the shapes of the curves are almost indistinguishable except for the high frequency noise probably caused by electrical pickup.

3.4.3 Effect of Vertical Position in Steel Plate

We expect the peak stress to decrease as pulses propagate up through the plate for two reasons. First, as the wave propagates it will diverge over a larger area. This effect should be expected to produce a decrease in peak stress inversely proportional to the square of the distance from the charge center for a spherical geometry. Second, since the relief wave following the peak stress will travel faster than the loading wave, the peak should decrease in magnitude even in the absence of divergence. This effect of finite amplitude waves should be more pronounced at higher stresses.

The three V-configuration experiments were undertaken to quantify the expectations just expressed. The results are shown graphically in Figures 21 and 22. In Figure 21, the decay with propagation is evident. From Figure 22 we can see that the decay goes approximately as the inverse square of the radius. It appears that the second mechanism of attenuation is unimportant for both spherical charges and pancake charges.

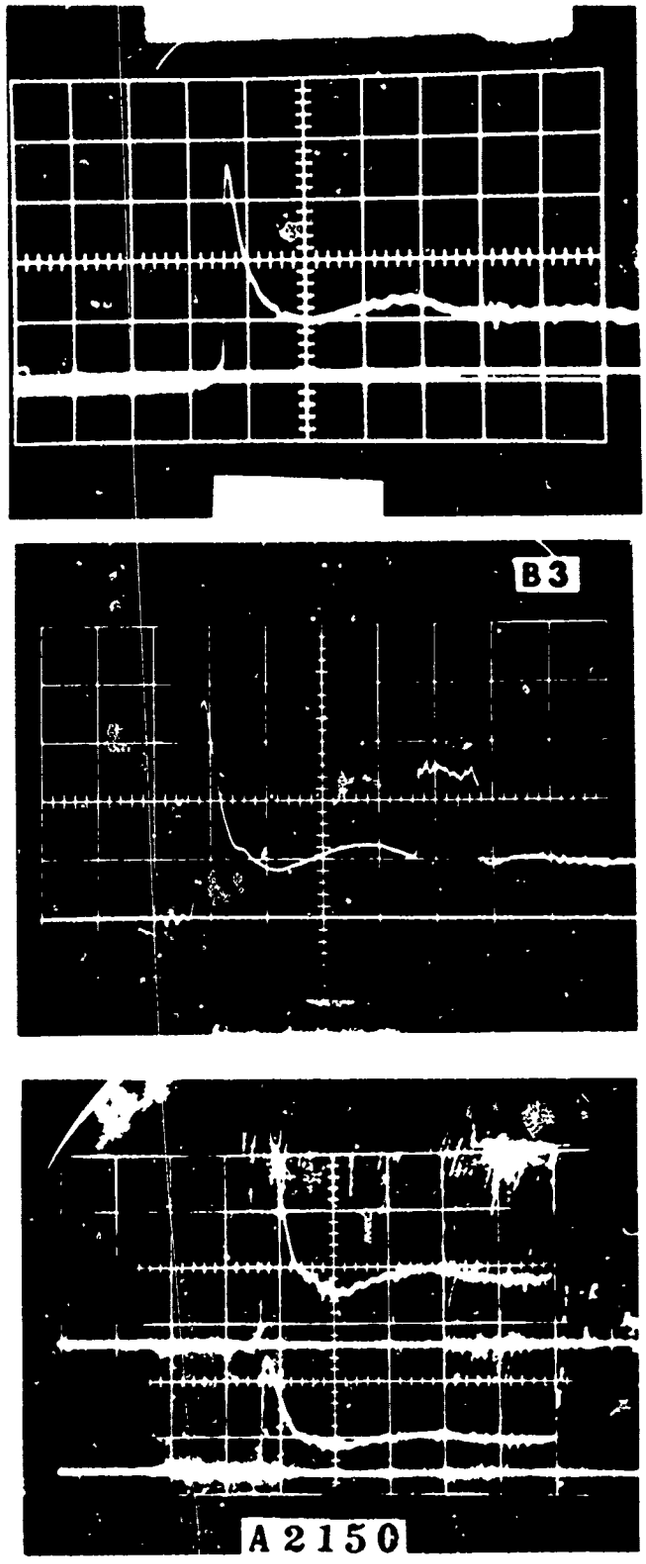

Figure 20. Example of reproducibility in experiments with pancake charges buried under dry soil. Peak stresses are 61 kbar, 69 kbar, and 68 kbar from top to bottom.

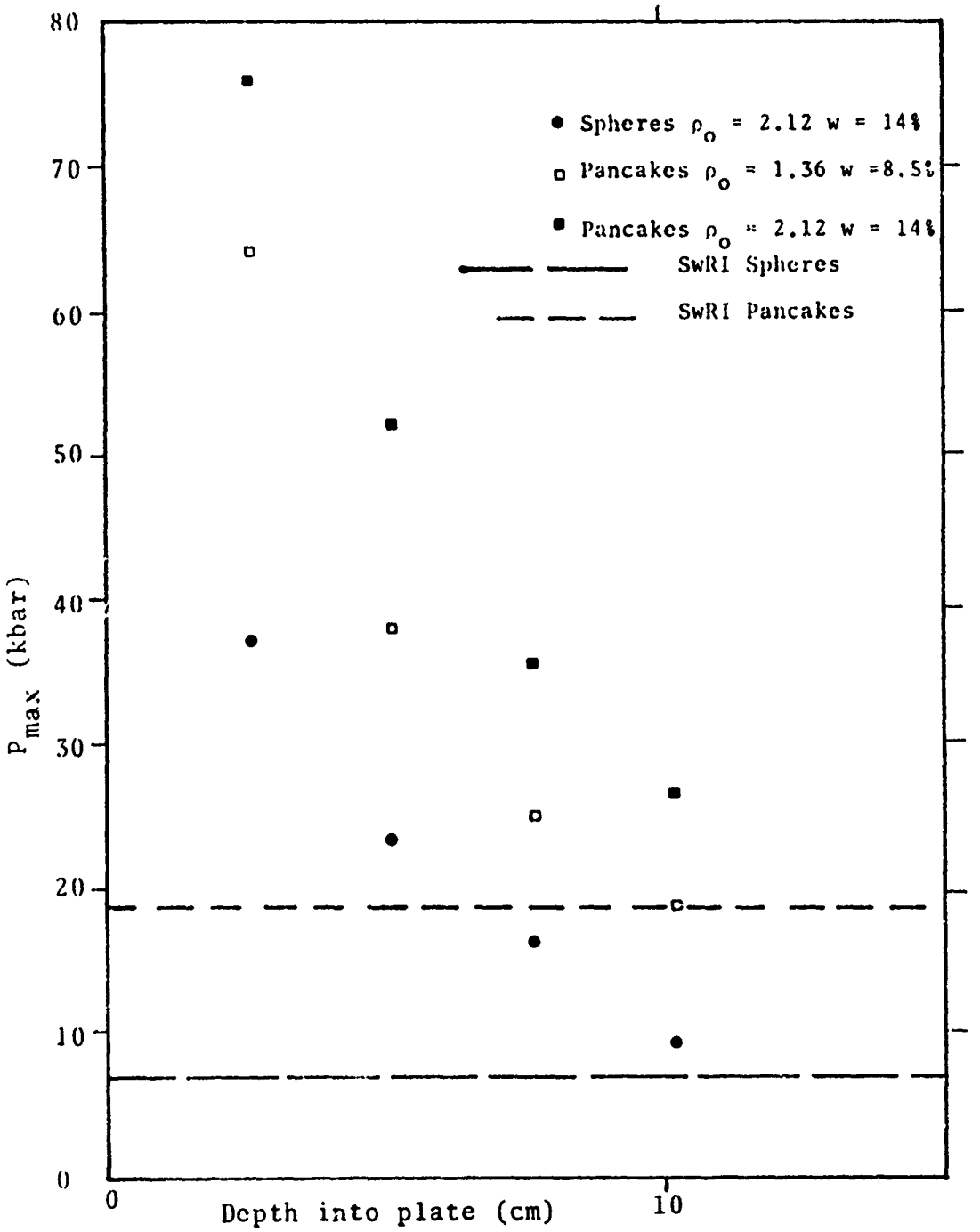

Figure 21. Decay of peak pressure with propagation distance in a steel plate above buried explosive charges.

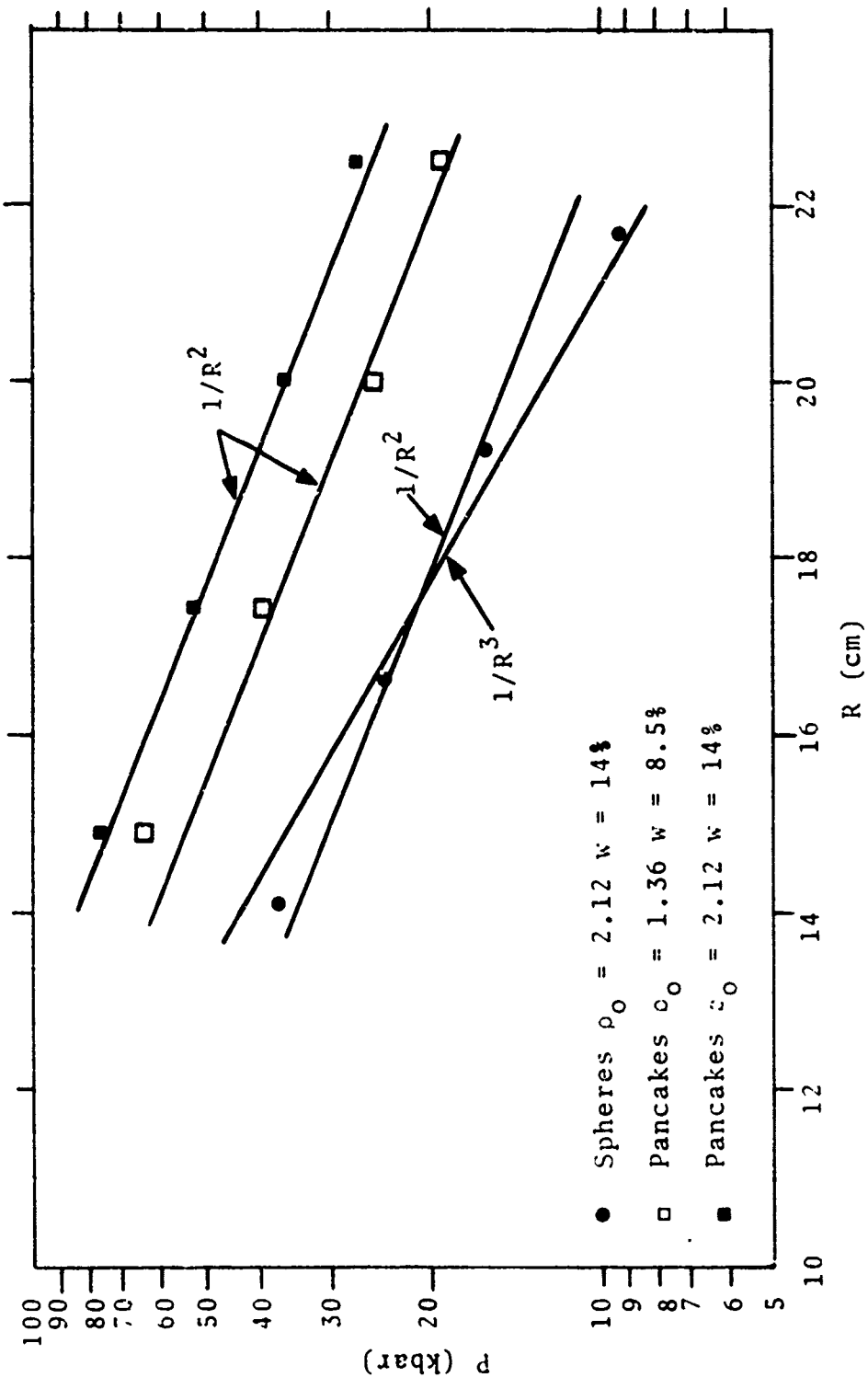

Figure 22. Decay of peak stress as in Figure 21 showing the approximate $1/R^2$ behavior.

Although we did not measure impulse directly in our experiments it can be determined from the area under a pressure-time curve. We note that the duration and shape of the main pressure pulse does not change significantly as the pulse propagates; however, the amplitude does decrease. Consequently, the specific impulse decreases on propagation in the same manner as the peak stress.

3.4.4 Dependence on Distance off Axis

The peak stress is a very sensitive function of the location of the gauge relative to the symmetry axis of the experiment. This is especially true for pancake charges. This can be clearly seen in Figure 23 where peak stress is shown as a function of the dimensionless variable r/R where r and R are the horizontal and vertical distances from the charge center respectively. This effect may account for most of the scatter in the data. An error in locating the plate over the charge axis of 1 cm can cause a change in the peak stress of as much as 25 percent of the peak stress directly above the charge.

It should be noted that all of the measurements reported here were taken at distances off axis of less than the charge diameter.

3.4.5 Effect of Soil State

As we mentioned in Subsection 3.1.2, Wenzel and Esparza[6] concluded that burial did little to increase peak stress from pancake charges (relative to charges detonated in air), but that the soil had a considerable effect for spherical charges. We argued that the mechanical impedance of the soil should be the important criterion leading to any difference

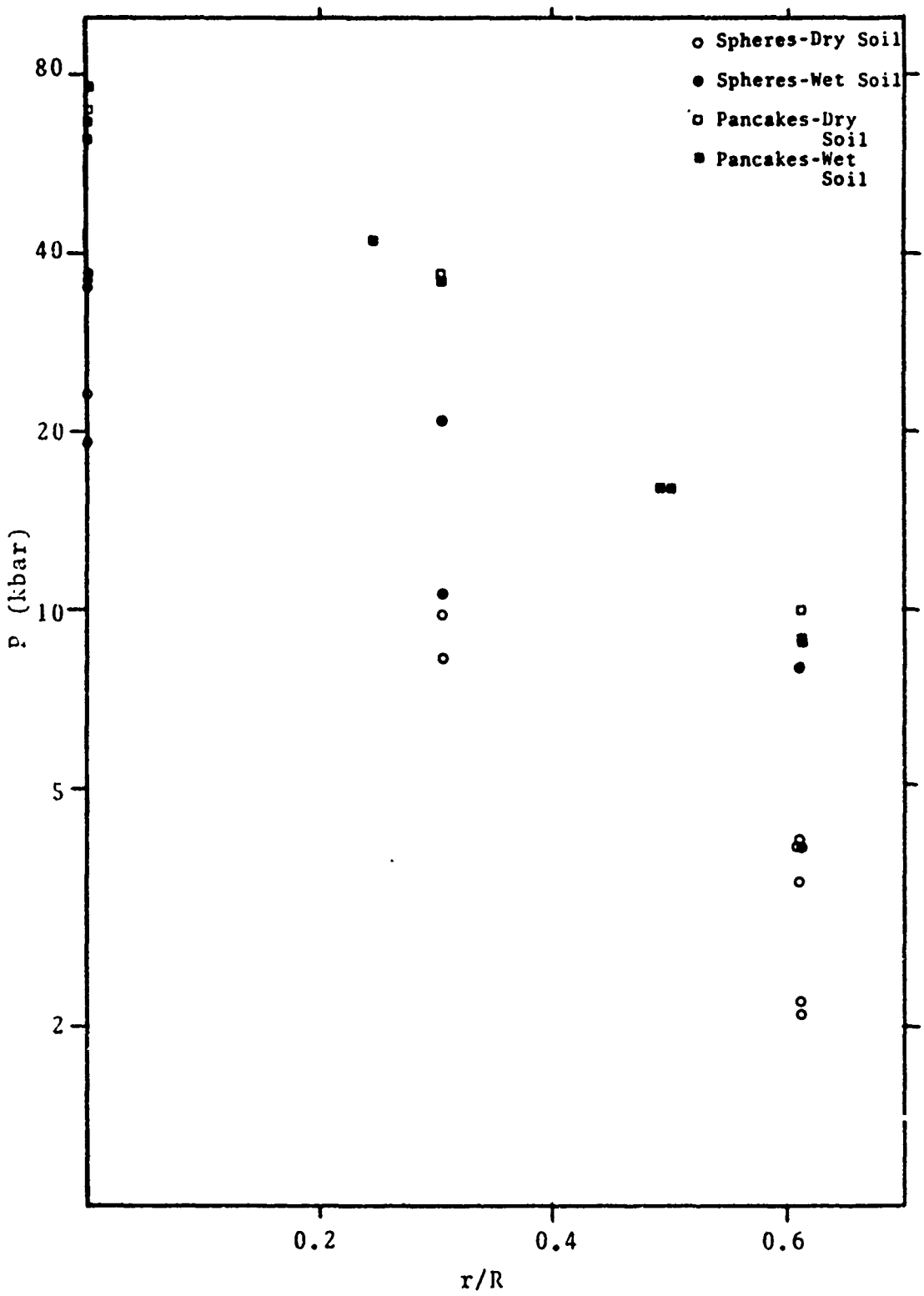

Figure 23. Dependence of peak stress on distance off axis (r) for buried explosive charges.

in peak stress for charges buried or in air. If this were true, we should expect to see a much greater peak stress for spherical charges under our "wet" soil than under our "dry" soil. Indeed, this is the case, as can be seen from Figure 23 and Table IV. For the pancake charges, on the other hand, we find no significant differences in peak stress, just as we would expect from the observations of Wenzel and Esparza.[6] These results, therefore, seem to confirm their observations and our explanation of them. This is at variance, however, with their observation that pancakes buried in mud produce much higher peak stresses than those in dry soil. The question of why we see no effect of burial of pancakes is not easy to answer, but if there is little difference between charges in air and those in dry soil, we should expect little variation between those in two different soils.

3.4.6 Comparison with Earlier Work

The broad features of the present work agree quite well with those seen by Wenzel and Esparza.[6] As just mentioned, our findings on the effects of different soils agree with theirs on soils versus air. Our study confirms the importance of soil impedance for spheres, as inferred by their modeling relations.

However, there is one glaring difference between their results and ours. That is the magnitude of the stresses involved. Stresses observed in the present study were uniformly about three times greater than those in corresponding experiments by Wenzel and Esparza.[6] The explosives used (C-4 in the present work, pentolite in the other) are not sufficiently different to account for this effect. The pulses seen in the earlier study were of much longer duration than those we saw. If we estimate the specific impulse at

the lower surface of the plate from our pressure-time data, we find that impulses are fairly close in the two sets of experiments.

We tentatively ascribe the differences to a combination of geometric dispersion and finite wave amplitude effects in the bar gauges. Note from our V configuration results of Figure 21 that our measurements at 4-inch depths in the plates give peak stresses close to the SwRI results. The different geometries of the plates and bars prevent any quantitative comparison of waveforms at a given distance from the impact surfaces. The bar gauges do not give a stress history that can be related to a particular depth in a plate. The 1-inch-deep manganin gauge results should be closer to impact stress.

3.5 SUMMARY AND CONCLUSIONS

Twelve experiments were carried out with spherical and pancake charges buried under wet and dry soils. In nine of these experiments stress histories were measured in a plane within a steel plate suspended over the charge. One of these gauges was directly over the charge and the others were located at various radii from the perpendicular axis through the plate from the charge center. In three of the experiments the stress histories were measured at four locations along the axis within the plate. Careful attention to soil preparation led to very good reproducibility of results.

The experimental investigations led to the following conclusions:

- The blast effect from a buried sphere of high explosive depends on the soil condition.
- The blast effect from a buried pancake of high explosive is independent of the soil condition.
- The peak stress and specific impulse fall off approximately as $1/R^2$ in a steel plate over a buried charge.
- The magnitude of peak stresses measured in the present study is about three times greater than those measured previously at SwRI. However, the impulses in the two studies are similar.

IV. CALCULATIONS

Three buried charge calculations were performed using a slightly modified version of the numerical model previously reported.[1,2] The additional modifications are reported in Appendix A. Calculation 1 involved a spherical charge and was modelled after Experiments 2115, 2132 and 2143 of Table IV. Calculation 2 involved a disc-shaped or pancake charge and was modelled after Experiments 2138, 2139 and 2144 of Table IV. Calculation 3 was not modelled after any of the experiments and involved a steel plate in contact with the soil surface. The results of these three calculations are reported here and comparisons with experiment are made whenever possible. For more details regarding the numerical model, Refs. 1 and 2 and Appendix A of this report should be consulted.

Figure 24 shows a typical initial configuration employed in the buried charge calculations. The values of depth-of-burial, D, and standoff, S, employed in the three calculations are given in Table V. Tracer particles, referred to as sensors in Figure 24, were placed at various positions throughout the steel plate for the purpose of monitoring the average axial normal stress components at those locations as a function of time and comparing the predicted results with experiment. In the calculations, rows of tracer particle sensors were placed along the front surface of the steel plate and at one-inch depth intervals. In the experimental set-up, gauges for measuring the stress were embedded in the plate at similar positions; however, no gauges were placed on the front of the plate since they would have been damaged by the impacting debris.

Figure 25 shows the predicted configuration of the high explosive charge, the soil and the steel plate at various times after initiation for a typical solution of the type that is of interest here. Since the configurational plots are quite similar and provide only qualitative information, they will not be repeated for each of the three solutions.

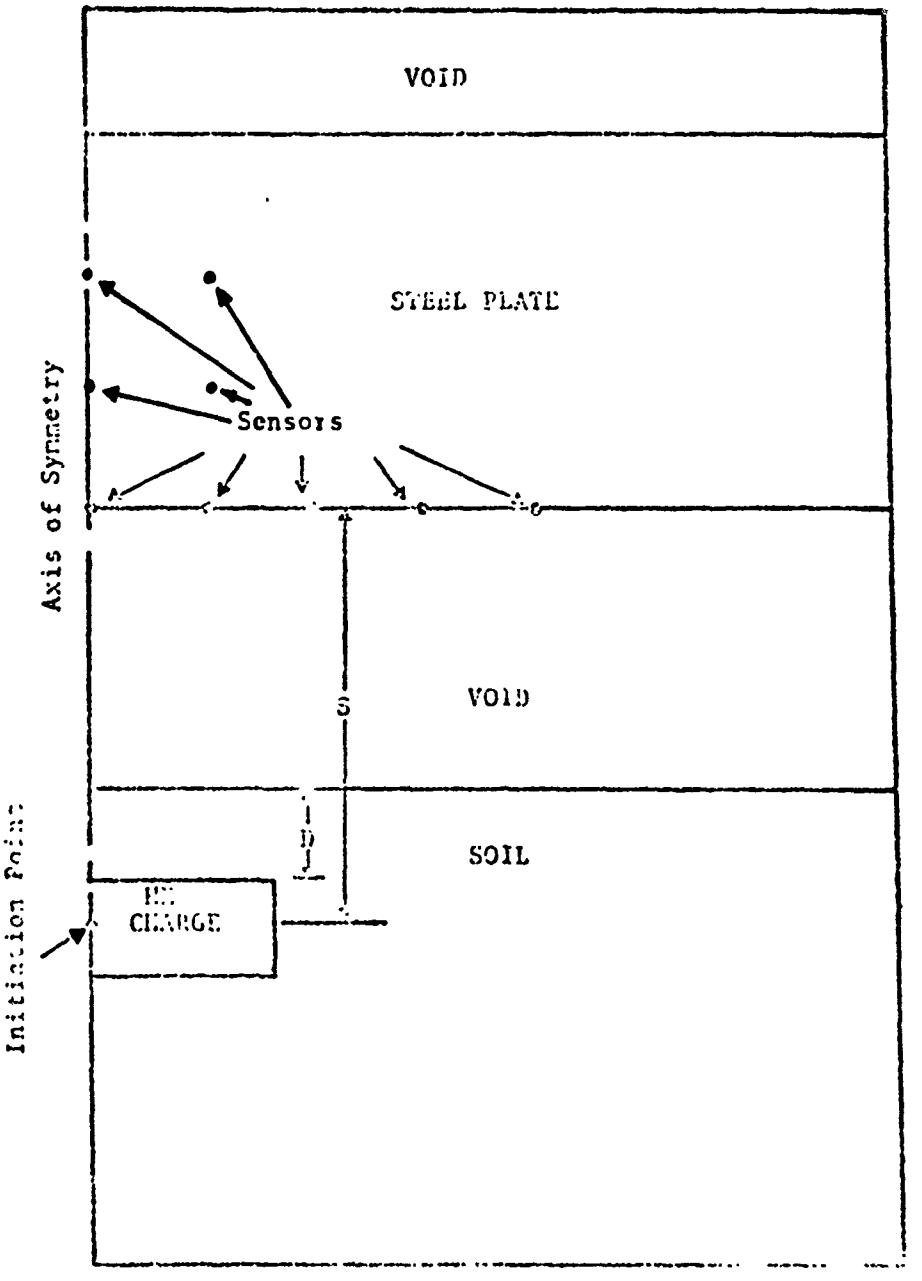

Fig. 24--Initial configuration for the class of problems of interest.

TABLE V

VALUES OF D AND S FOR THE THREE CALCULATIONS

Calculation Number	Experimental Identification Numbers	Charge Configuration	Depth of Burial, D (cm)	Standoff, S (cm)
1	2115,2132,2143	Spherical	2.54	11.51
2	2138,2139,2144	Pancake	2.54	12.50
3	------	Pancake	2.54	4.88

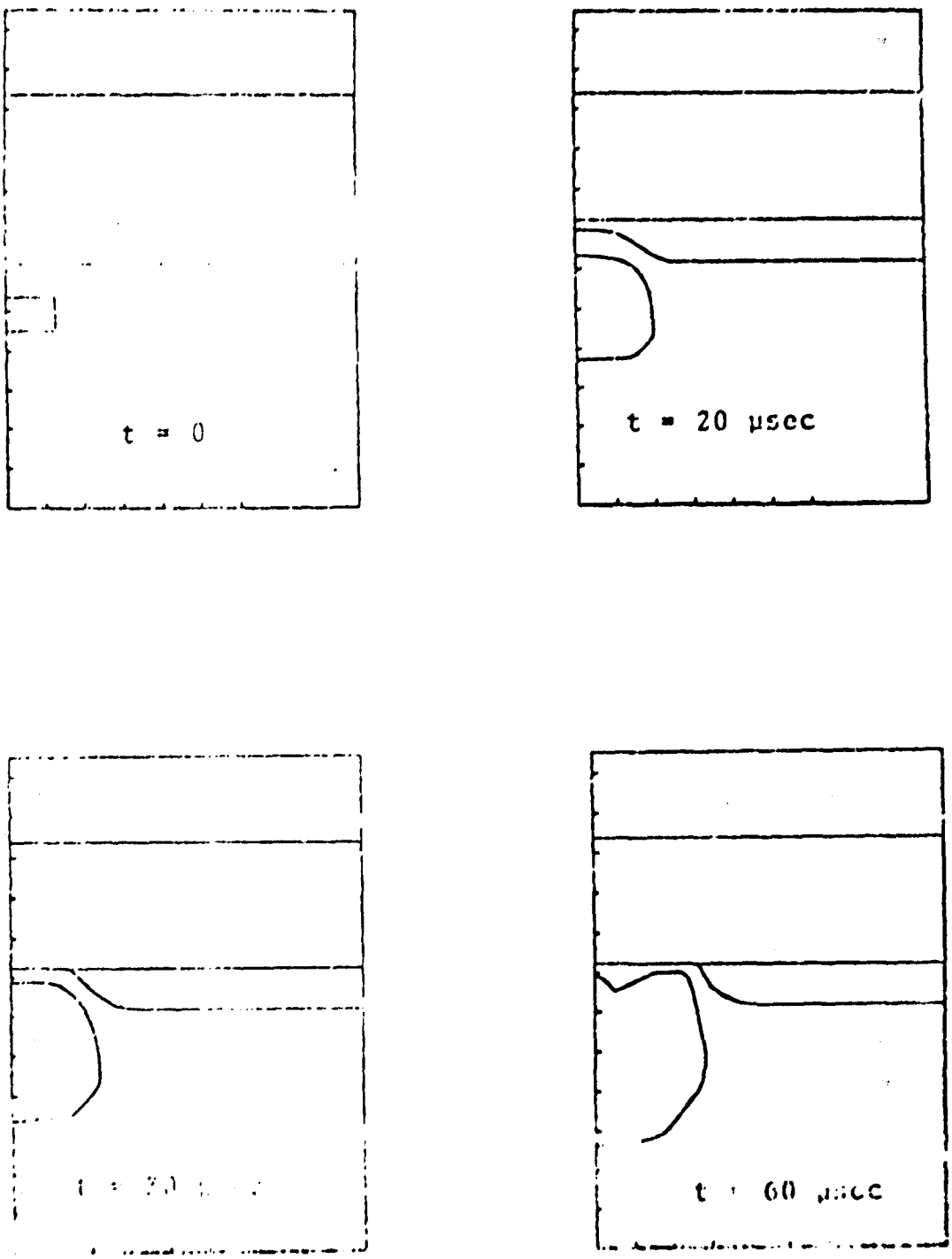

Fig. 25--Configurations at various times after initiation for a typical buried mine-steel plate interaction calculation.

The predicted total normal axial stress pulse as a function of distance into the plate is shown at various times in Figure 26 for Calculation 1 of Table V. Initiation of the buried charge occurred at t = 0.

Figure 27 is a plot of the predicted axial stress history, $\sigma_{yy}(t)$, at the front surface of the steel plate and at various gage locations within the plate. It is seen in Figure 27 that the stress pulse attenuated quite rapidly as it propagated into the plate. The symbols, (x), in Figure 27 show the experimentally measured peak stresses at the various gage locations. It is seen that agreement between theory and experiment is quite good.

In Figure 28 the predicted axial stress histories, $\sigma_{yy}(t)$, at gages located one inch into the plate and at various radial distances, r, are shown for Calculation 1. The experimental data points given by the symbol (x) indicate the measured peak stresses at the various gage locations. As is seen from Figure 28, while there is some spread in the experimental data, agreement between theory and experiment is quite good.

Stress plots similar to those shown in Figures 26 through 28 are provided in Figures 29 through 31 for Calculation 2 of Table V. In addition to those plots, stress histories at gages located two inches deep in the steel plate are provided for Calculation 2 in Figure 32. As seen in Figure 30 the predicted stress attenuation through the thickness of the plate is in good agreement with the measured stress attenuation; however, the predicted stress peaks are consistently lower than the measured values by a few per cent.

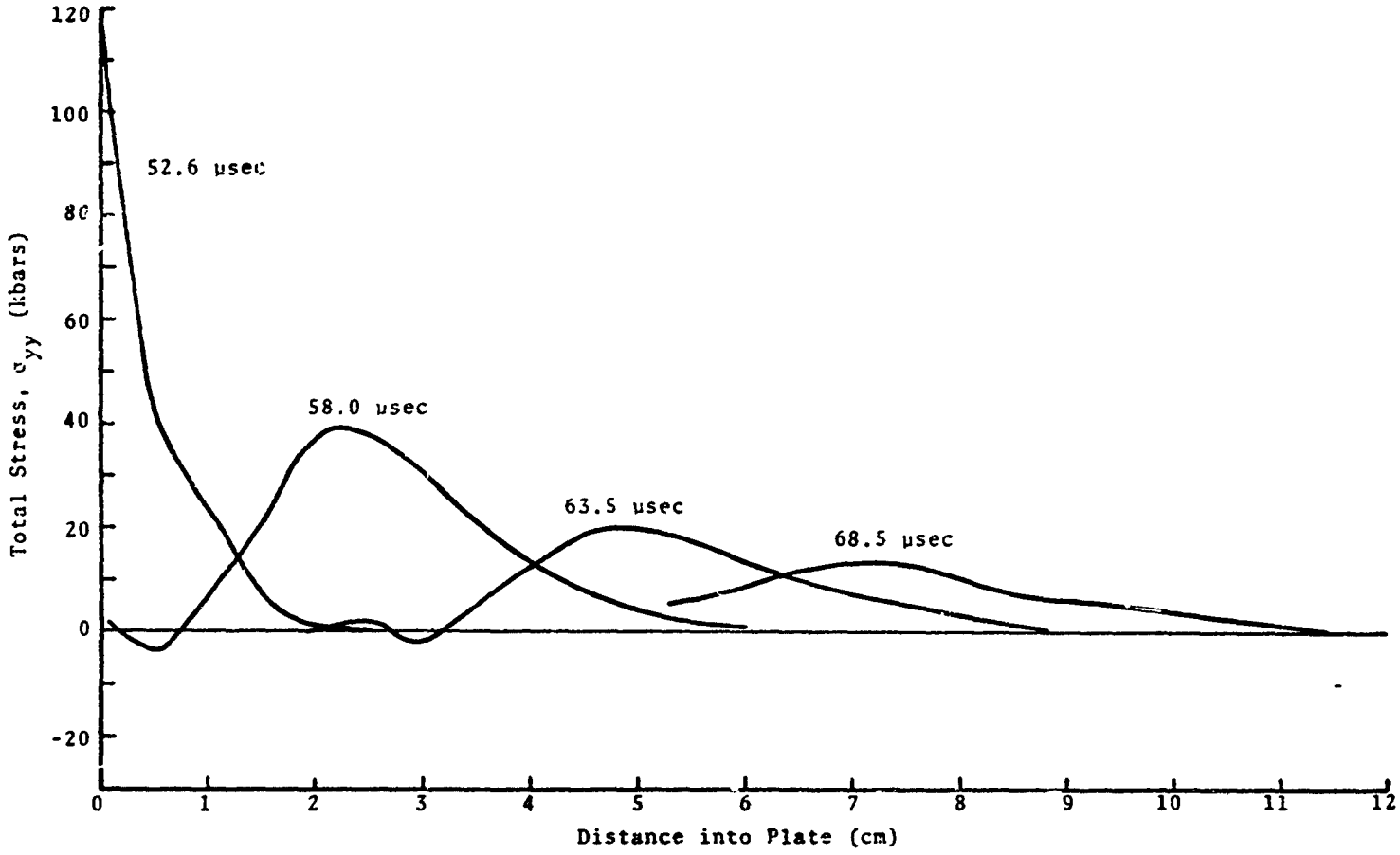

Figure 26. Predicted total normal axial stress pulse as a function of distance into the plate at various times after charge initiation for calculation 1.

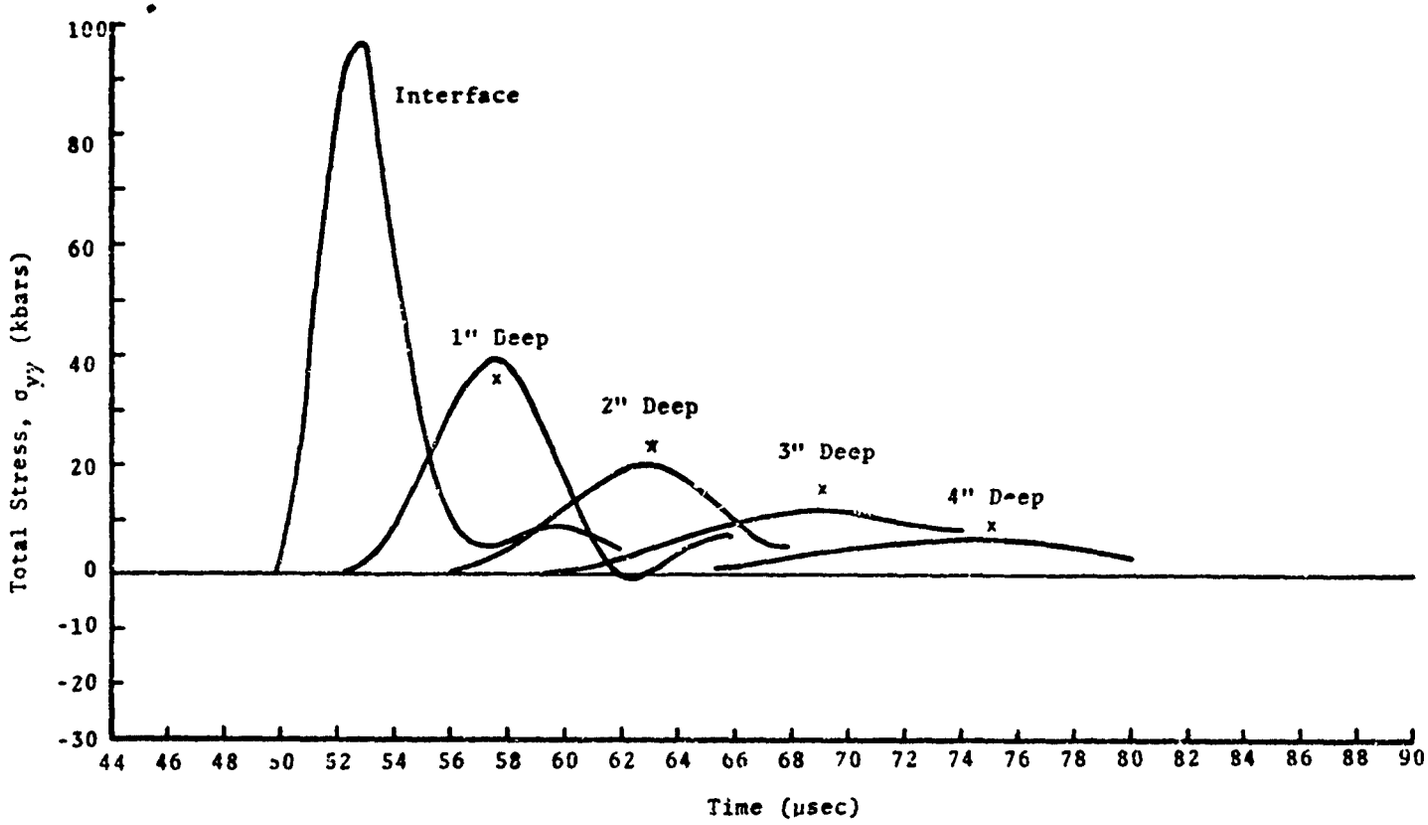

Figure 27. Plot of predicted axial stress history, $\sigma_{yy}(t)$, at the front surface of the steel plate and at various gauge locations for Calculation 1. The experimentally measured values are shown by the symbol (x).

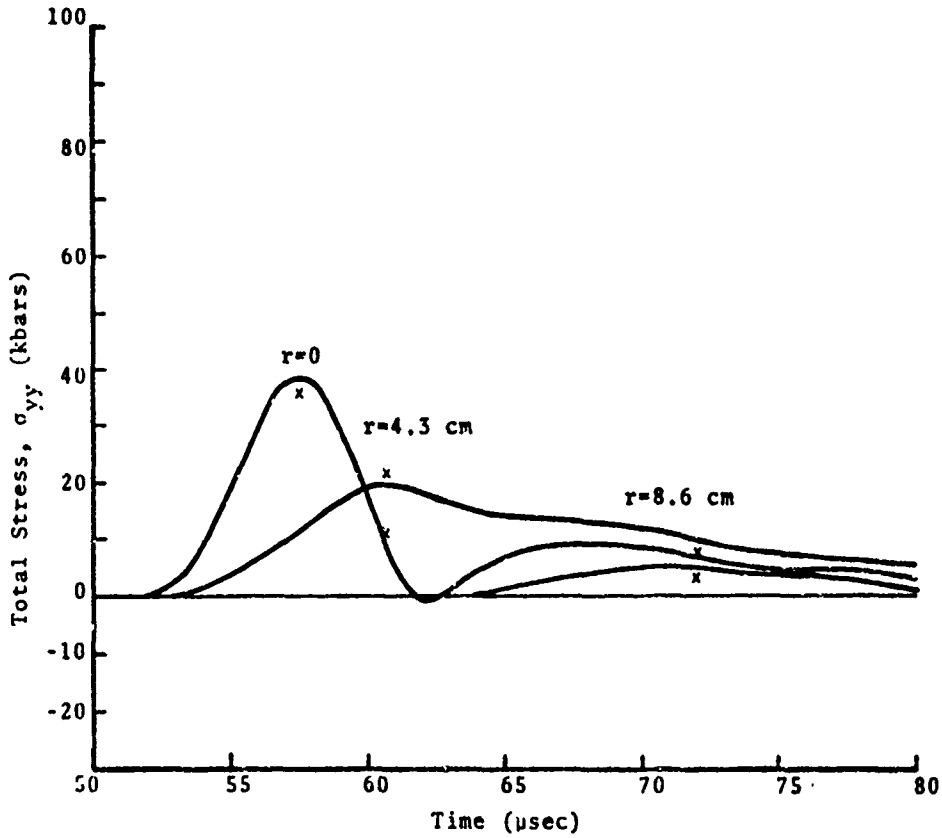

Figure 28. Plot of predicted axial stress history, $\sigma_{yy}(t)$, at gauges located one inch into the plate and at various radial distances, r, for Calculation 1. The experimentally measured values are shown by the symbol (x).

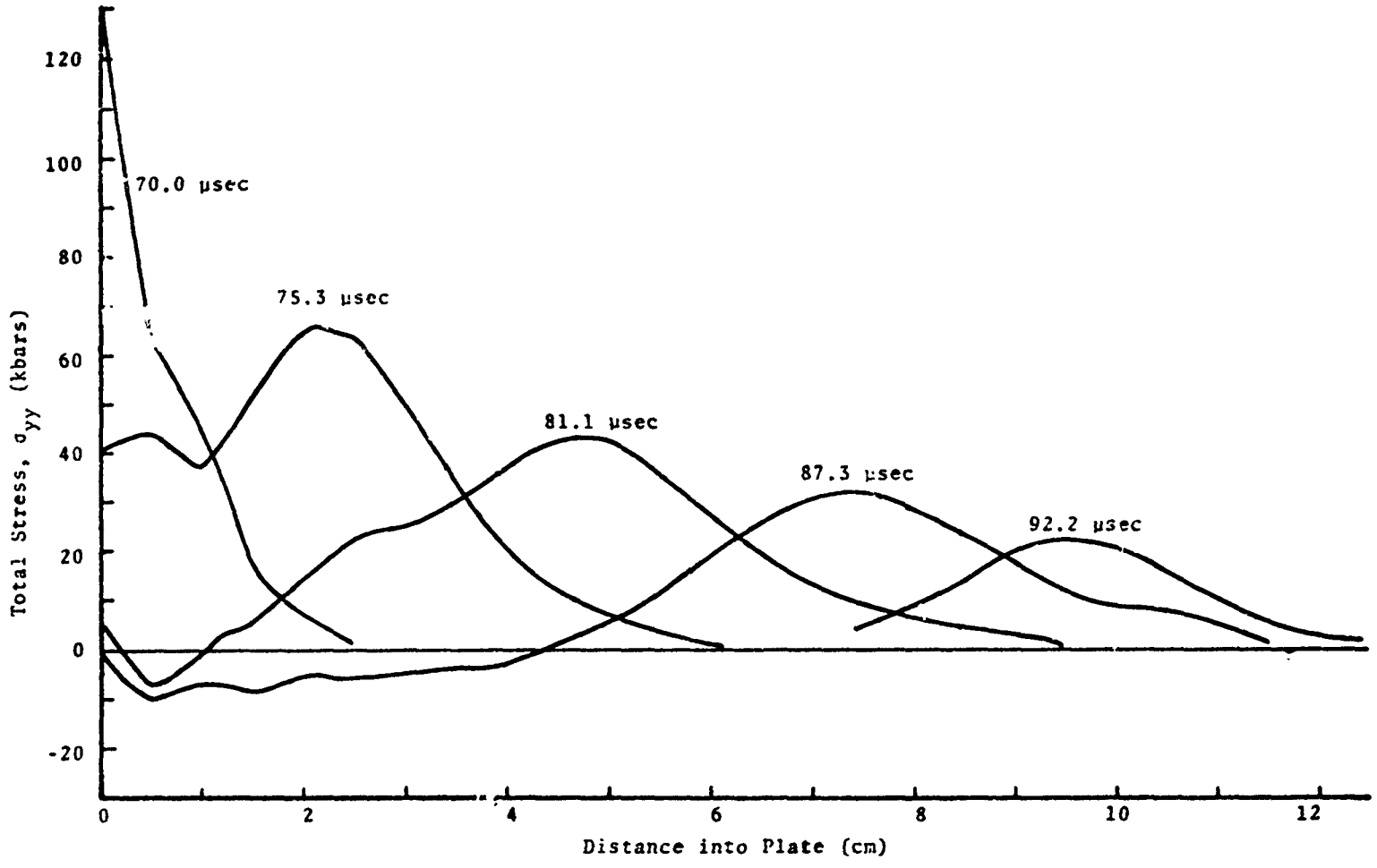

Figure 29. Predicted total normal axial stress pulse as a function of distance into the plate at various times after charge initiation for Calculation 2.

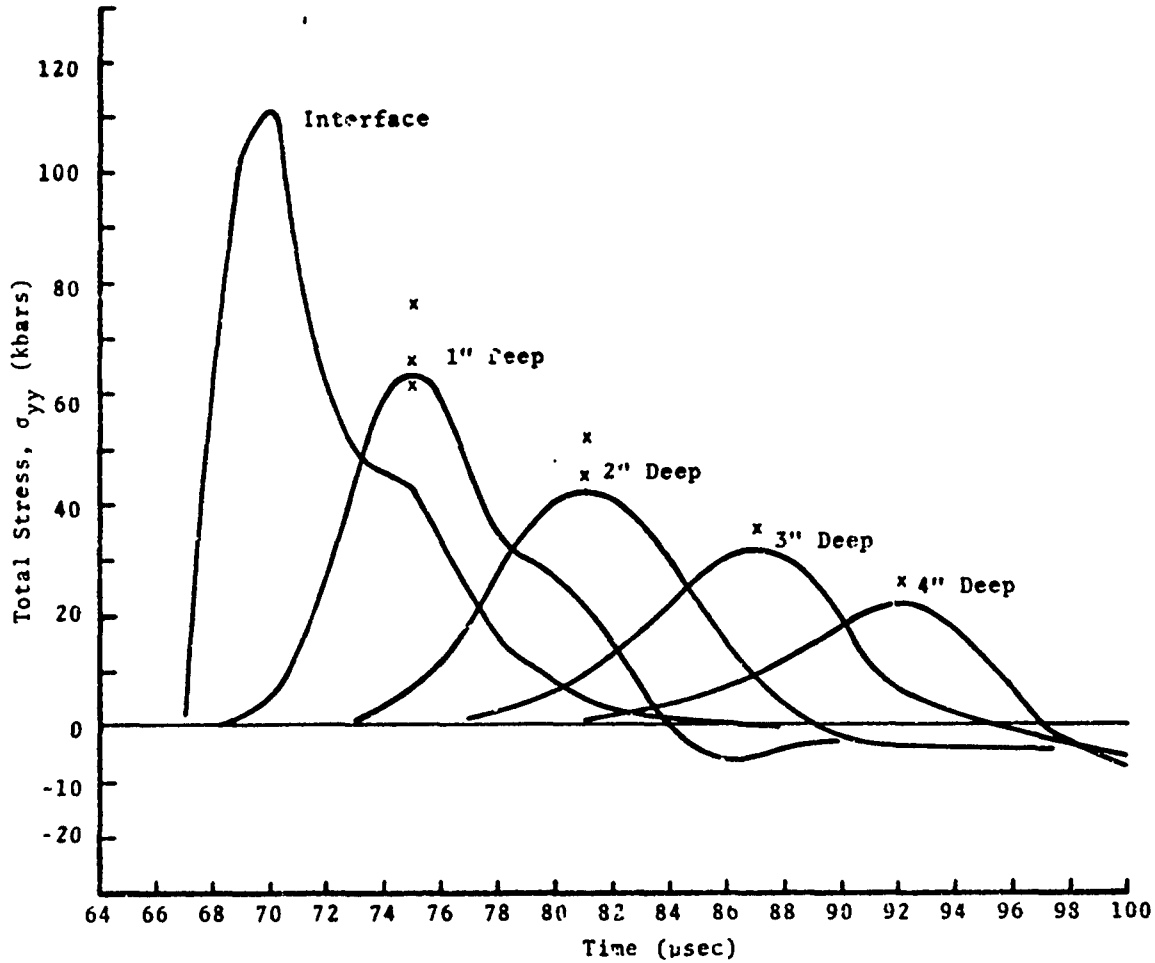

Figure 30. Plot of predicted axial stress history, $\sigma_{yy}(t)$, at the front surface of the steel plate and at various gauge locations for Calculation 2. The experimentally measured values are shown by the symbol (x).

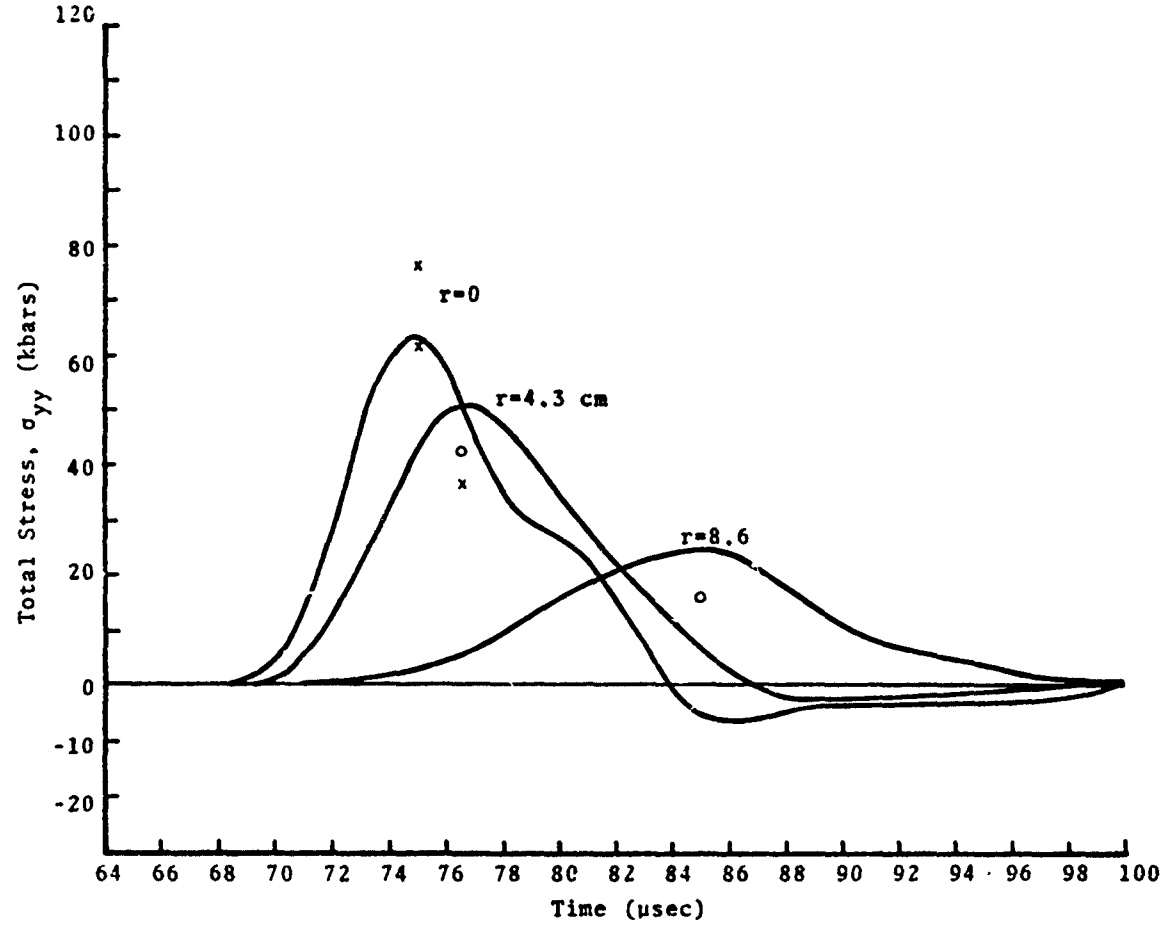

Figure 31. Plot of predicted axial stress history, $\sigma_{yy}(t)$, at gauges located one inch into the plate and at various radial distances, r, for Calculation 2. The experimentally measured values are shown by the symbol (x) and values extrapolated as noted in Table IV are shown by the symbol (o).

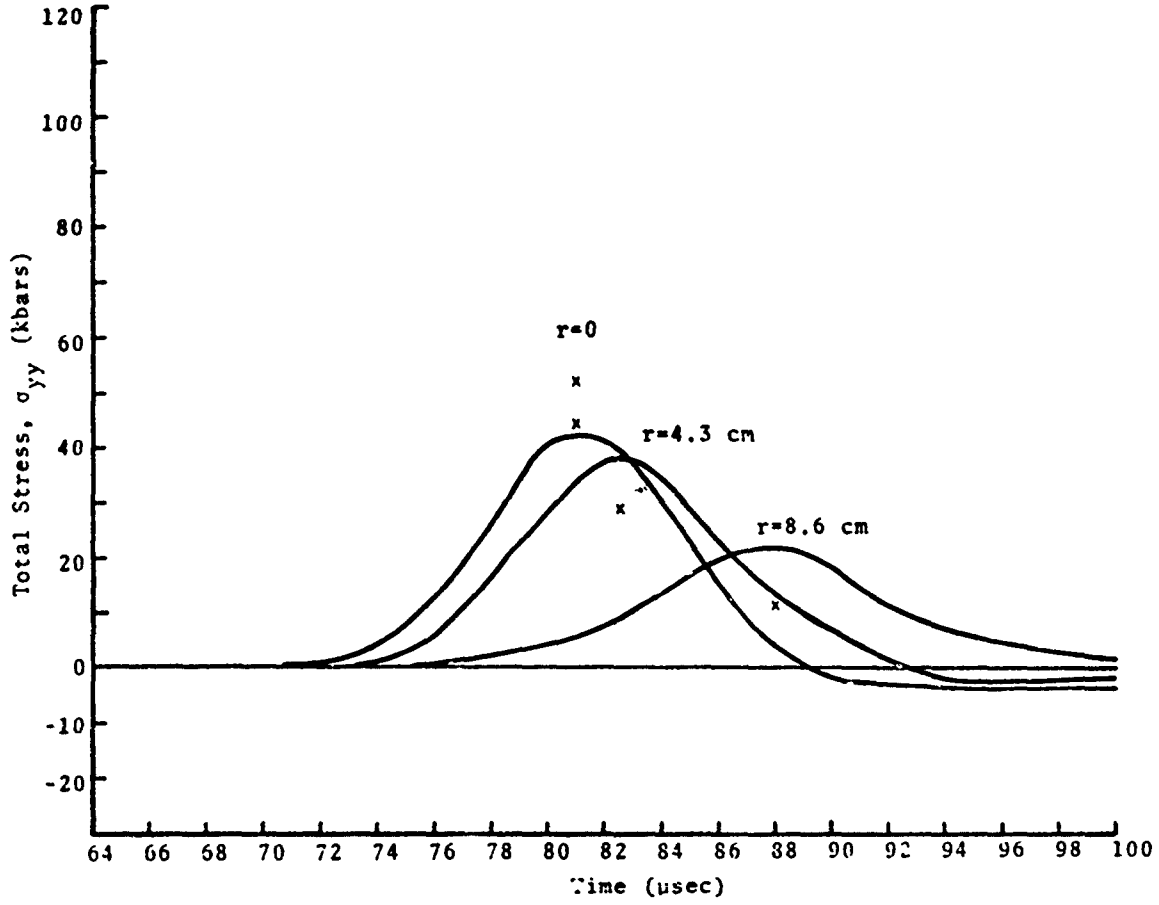

Figure 32. Plot of predicted axial stress history, $\sigma_{yy}(t)$, at gauges located two inches into the plate and at various radial distances, r, for Calculation 2. The experimentally measured values are shown by the symbol (x).

The predicted axial stress attenuation in the radial direction for Calculation 2 does not agree as well with experiment as does the attenuation through the plate. As seen in Figures 31 and 32, the predicted radial attenuation is not as great as the measured values. The reason for this difference in the theoretical and experimental curves for the radial attenuation of the peak axial stress components for Calculation 2 is not completely understood at this time; however, it is apparent from the last plot in Figure 3 that the predicted debris momentum did not decrease monotonically in the radial direction.

Calculation 3 involved a steel plate in contact with the ground and the predicted total normal axial stress as a function of distance into the plate is plotted at various times after charge initiation in Figure 33. Figure 34 shows the predicted attenuation of the peak stress as the wave propagates through the plate. The experimental matrix did not include a configuration similar to Calculation 3 so that no data are currently available for comparison with the predicted peak stresses. Figures 35 and 36 show the attenuation of the axial stress wave as it propagates into the plate at radial distances of 1.8 and 3.7 cm, respectively, for Calculation 3. While no experimental data were available for comparison with the results of Calculation 3, these results were, however, compared with results obtained at MERDC[21] in which the Lagrangian code TOODY[22] was employed. The predicted values of the impulse delivered to the steel plate along the axis of symmetry differed by only 3.7%[21].

The predicted total momentum given to the steel plate as a function of time after debris impact is plotted in Figure 37 for each of the three calculations of Table V.

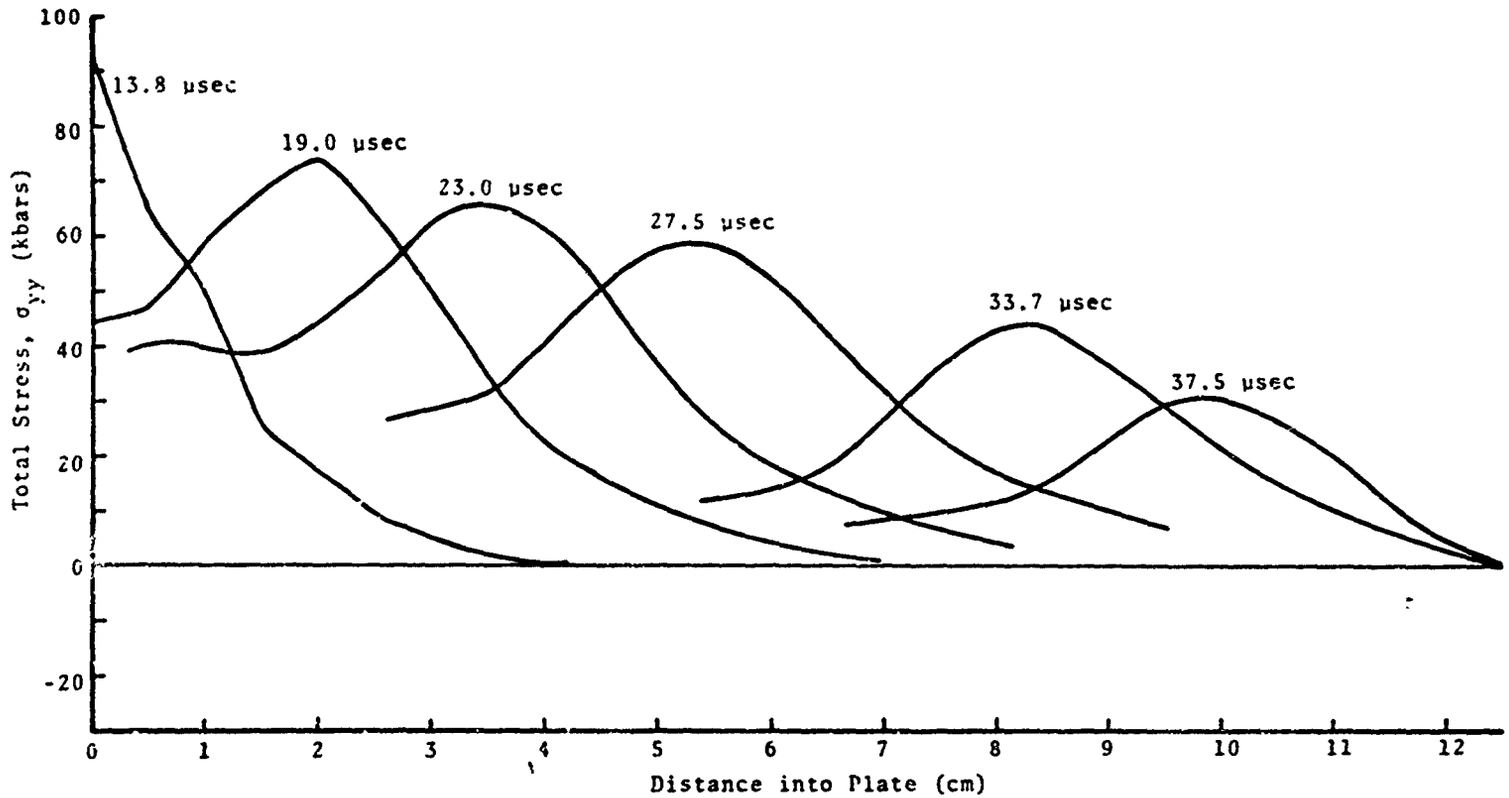

Figure 33. Predicted total normal axial stress pulse as a function of distance into the plate at various times after charge initiation for Calculation 3.

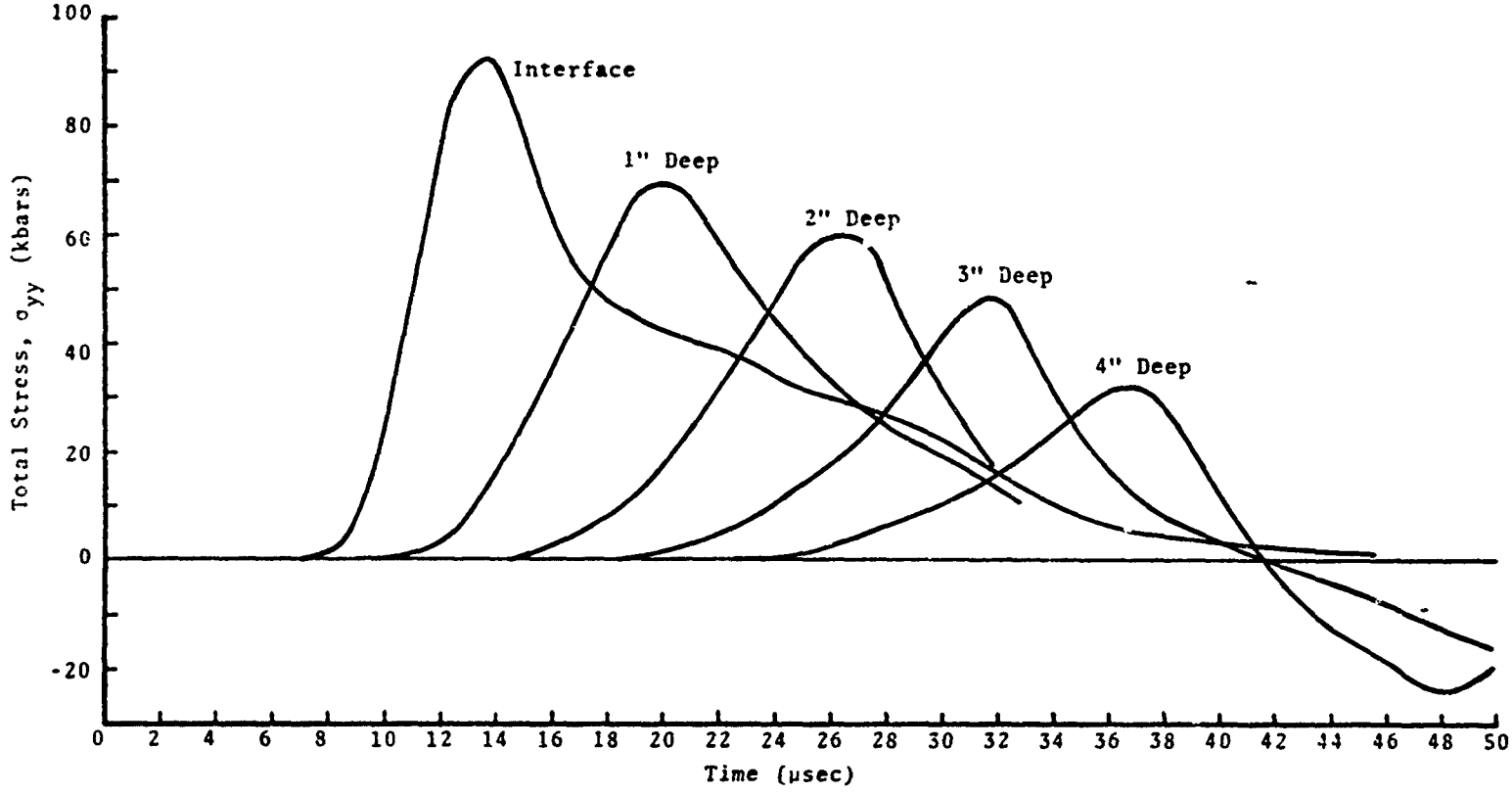

Figure 34. Plot of predicted axial stress history, $\sigma_{yy}(t)$, at the front surface of the steel plate and at various gauge locations for Calculation 3.

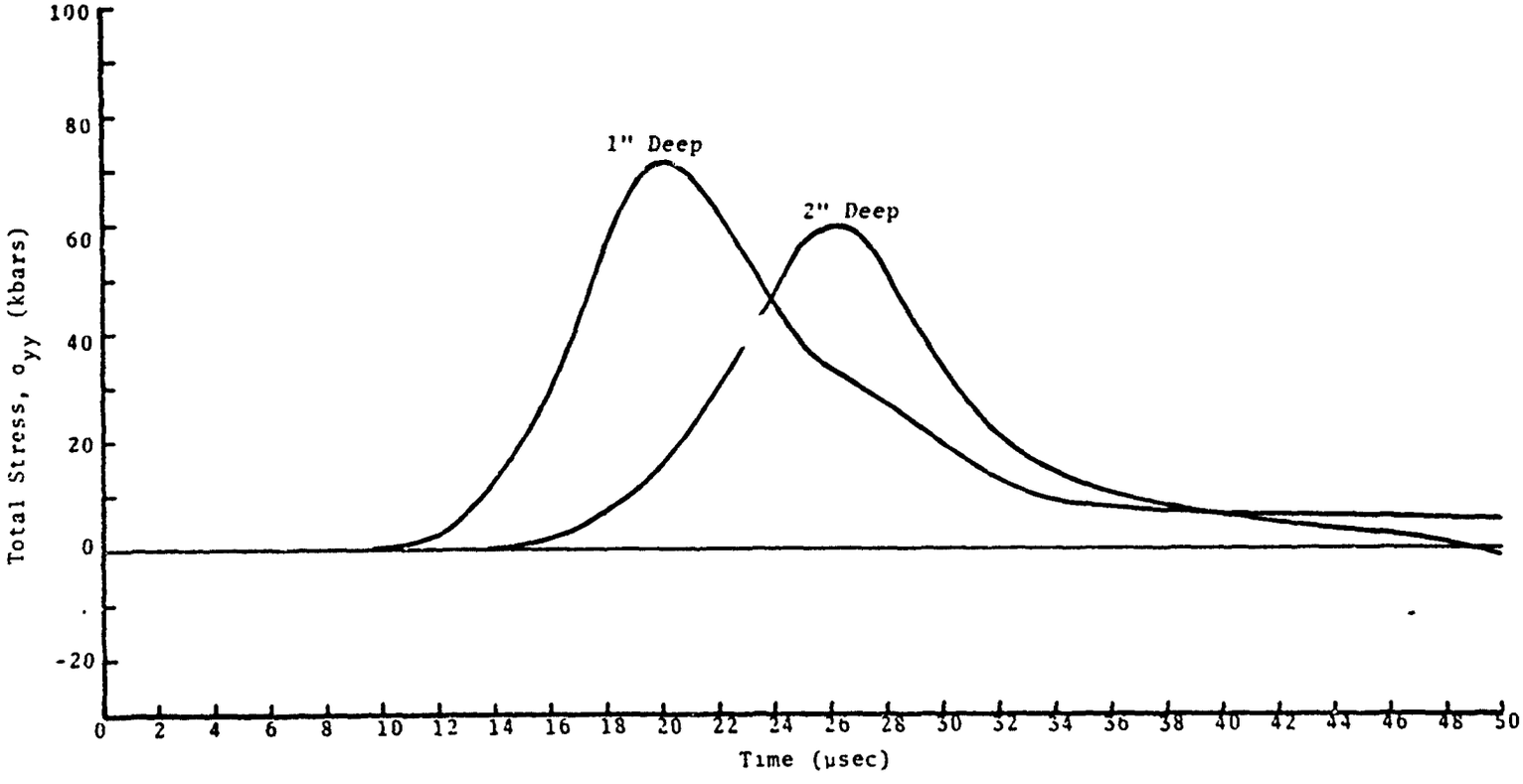

Figure 35. Plot of predicted axial stress history, $\sigma_{yy}(t)$, for gauges located 1.8 cm from the axis of symmetry for Calculation 3.

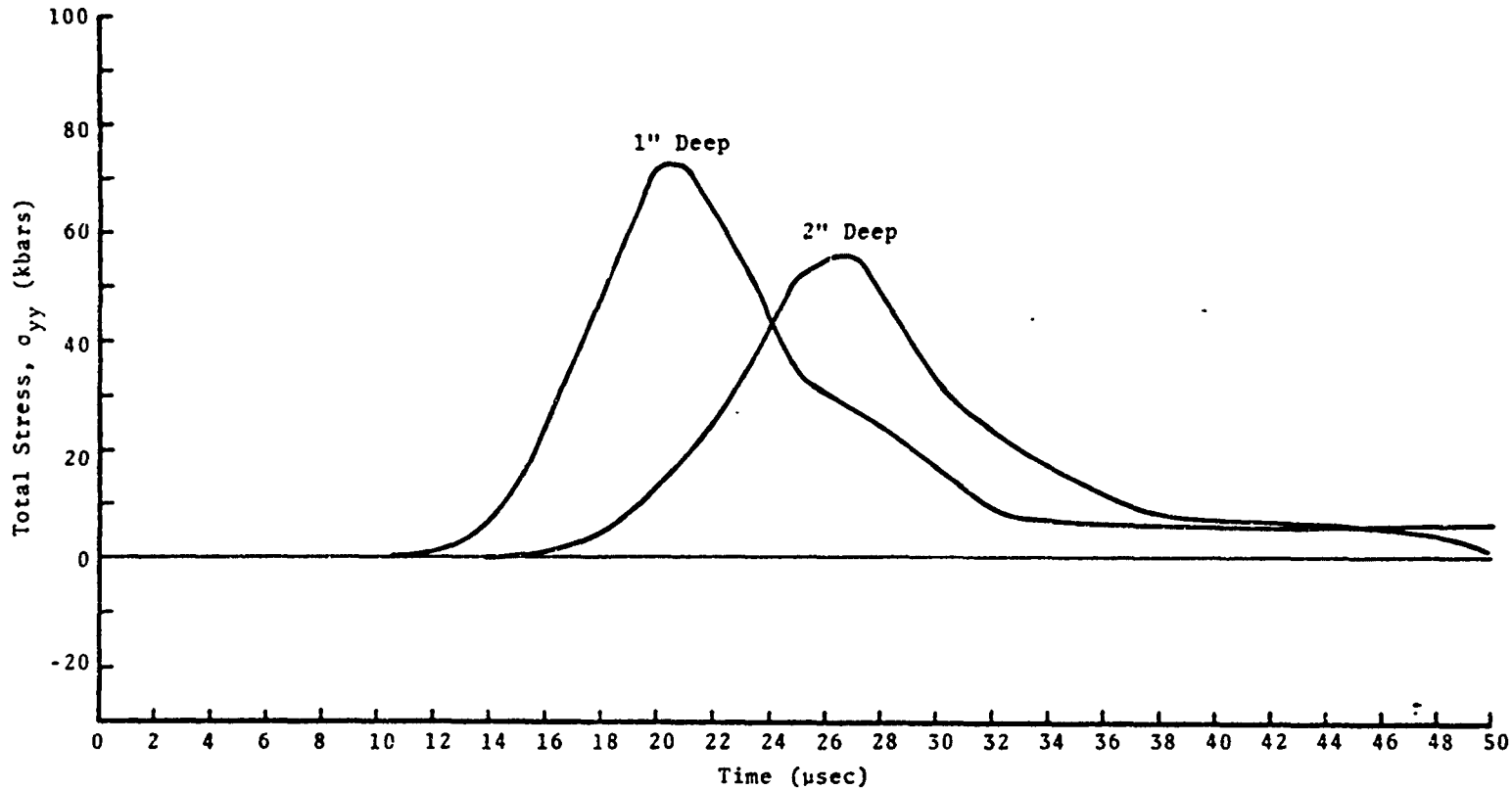

Figure 36. Plot of predicted axial stress history, $\sigma_{yy}(t)$, for gauges located 3.7 cm from the axis of symmetry for Calculation 3.

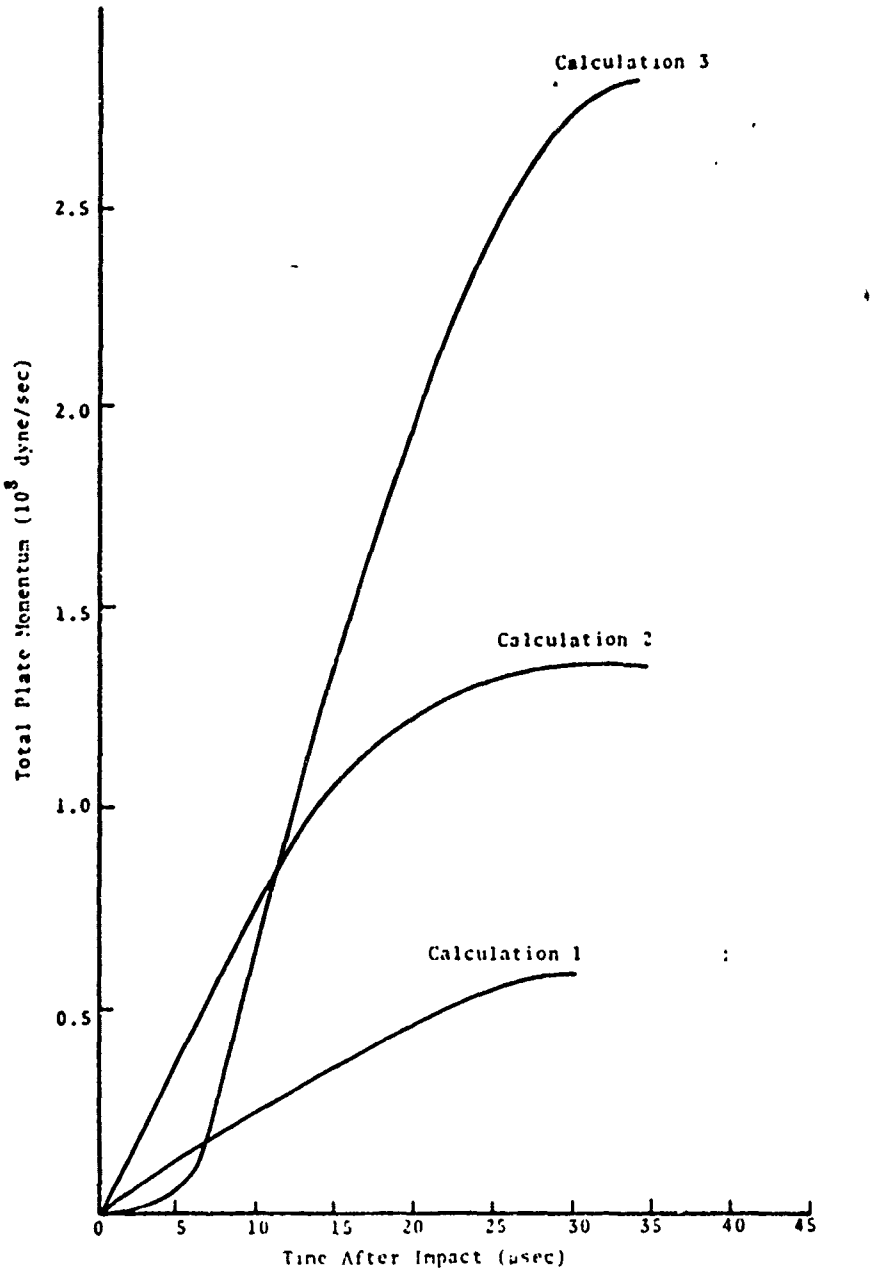

Figure 37. Plot of total plate momentum as a function of time after debris impact for Calculations1 through 3.

V. CONCLUSIONS

Numerical techniques have been developed and proven successful for predicting the effects of buried mines on simple structures located above the ground. Experimental techniques for determining dynamic material properties of soils have been employed to obtain equation of state parameters which are necessary as part of the input to the numerical model.

Three two-dimensional calculations were performed. In these calculations the buried charges were detonated, the expanding detonated products accelerated the soil and the debris impacted a steel plate located above ground level. The stress distributions throughout the steel plates as a function of time after charge initiation were determined and compared with data from actual tests. The agreement between theory and experiment was quite good.

Specific conclusions regarding the results of the dynamic soil properties tests and the actual buried charge-steel plate interaction tests are listed at the ends of Sections II and III, respectively.

In general it can be said that the combined theoretical-experimental program has significantly advanced the state-of-the-art of predictive techniques related to the effects of buried charges on simple, above-ground structures.

11. Ahrens, T. J. and E. S. Gaffney, "Dynamic Compression of Enstatite," J. Geophys. Res., 76 (23), 5504-5513 (1971).

12. Ahrens, T. J., J. H. Lower and P. L. Lagus, "Equation of State of Forsterite," J. Geophys. Res., 76, (2), 518-528 (1971).

13. Ahrens, T. J. and E. H. Graham, "A Shock-Induced Phase Change in Iron-Silicate Garnet," Earth and Planet. Sci. Letters, 14, 87-90 (1972).

14. Hoffman, A. J. and S. N. Mills, Jr., "Air Blast Measurements about Explosive Charges at Side-On and Normal Incidence," BRL Report No. 988 (1956).

15. Goodman, H. J., "Compiled Free-Air Blast Data on Bare Spherical Pentolite," BRL Report No. 1092 (1960).

16. Jack, W. H., Jr., and B. F. Armendt, Jr., "Measurements of Normally Reflected Shock Parameters from Explosive Charges under Simulated High Altitude Conditions," BRL Report No. 1280 (1965).

17. Cockrell, J. K., R. Anderson, et al., "Phase III Parametric Design/Cost Effectiveness Study for a Mechanical Infantry Combat Vehicle (MICV) (U)," Cornell Aeronautical Lab, Report 6M-2144-H-4 (Conf.) (1968).

18. Wenzel, A. B., R. C. Young and C. R. Russell, "Structural Response and Human Protection from Land Mines (U)," Allison Division, General Motors Corp., Cleveland Army Tank-Automotive Plant, TR 3481 (S) (1968).

19. Kinchelce, W. L.,"Reduction of Blast Effects," Final Quarterly Report 0477-01(04)FP, Contract DA-44-009-ENG-4780 (1962).

20. Dove, R. C. and P. H. Adams, Experimental Stress Analysis and Motion Measurements, Merrill, Columbus, Ohio (1964).

21. Morris, B., "Measurement of Phenomena Associated with the Detonation of Shallow Buried Explosives," International Symposium on Shock Analysis and Testing, 16-18 Oct 1974, proceedings to be published.

22. Bertholf, L. D. and S. E. Benzley, "TOODY II. A Computer Program for Two-Dimensional Wave Propagation," Sandia Laboratories Research Report SC-RR-68-41 (Nov. 1968).

APPENDIX A

HELP CODE MODIFICATIONS

Some changes have been made to the version of the HELP code reported in Reference 2. The major change has been to incorporate an improved artificial viscosity formulation. The artificial viscosity which is added to the stress at the boundaries between neighboring cells K and K1 is of the form $Q=QLIN\cdot\bar{\rho}\cdot\bar{C}\cdot\Delta V$, where QLIN is an input parameter, $\bar{\rho}$ = 0.5 (ρ(K) + ρ (K1)) where ρ is the cell density, $\bar{C}$ = 0.5 (C(K) + C (K1)) where C is the cell sound speed, and ΔV is the velocity difference between the two cells. For the top boundary the velocity difference is ΔV = V(K) - V(K1) where V is the cell axial velocity, while for the right boundary it is ΔV = U(K) - U (K1) where U is the cell radial velocity.

This formulation has required the addition of a function, SNDSPD, which calculates the cell sound speed. For the high explosive package the sound speed is given by $C=\sqrt{\gamma(\gamma-1)E}$, where E is the specific internal energy and γ is an input parameter. For other materials the sound speed is given by $C = C_0 + 0.5\sqrt{P}$, where P is the cell pressure and C_0 is the bulk sound speed. For mixed cells, a volume weighted average is used.

Two input variables have been added to the Z block. The first of these, in location 11, is QLIN, the artificial viscosity coefficient. The other is an integer, NVRTE, in location 107. This variable must be defined equal to NVRTEX in the initial problem setup.

Another code modification was made in order to reduce the zoning requirements in the vicinity of the debris-steel plate interface. In the unmodified version of the code, the under-dense soil entering the mixed, interface cell during the transport phase transferred momentum to the plate

for several cycles before a significant stress gradient acted across the interface. The result of this lack of synchronization was to artifically broaden the stress pulse delivered to the plate. This problem could have been eliminated by choosing finer zoning; however, the cost of the calculations would then have been significantly greater. The modification that was made simply inhibited the transport into the steel cells until a significant stress gradient developed across the interface so that the Phase II (mass transport) and Phase III (stress gradient) effects would be synchronized.